


1991

Neural network approach for solving inverse problems

Ibrahim Mohamed Elshafiey
Iowa State University

Follow this and additional works at: <https://lib.dr.iastate.edu/rtd>

 Part of the [Artificial Intelligence and Robotics Commons](#), [Other Electrical and Computer Engineering Commons](#), and the [Theory and Algorithms Commons](#)

Recommended Citation

Elshafiey, Ibrahim Mohamed, "Neural network approach for solving inverse problems" (1991). *Retrospective Theses and Dissertations*. 16966.
<https://lib.dr.iastate.edu/rtd/16966>

This Thesis is brought to you for free and open access by the Iowa State University Capstones, Theses and Dissertations at Iowa State University Digital Repository. It has been accepted for inclusion in Retrospective Theses and Dissertations by an authorized administrator of Iowa State University Digital Repository. For more information, please contact digirep@iastate.edu.

**Neural network approach for
solving inverse problems**

by

Ibrahim Elshafey

A thesis Submitted to the
Graduate Faculty in Partial Fulfillment of the
Requirements for the Degree of
MASTER OF SCIENCE

Department: Electrical Engineering and Computer Engineering
Major: Electrical Engineering

Signatures have been redacted for privacy

Iowa State University
Ames, Iowa
1991

Copyright © Ibrahim Elshafey, 1991. All rights reserved.

TABLE OF CONTENTS

CHAPTER 1. INTRODUCTION	1
CHAPTER 2. INVERSE PROBLEMS	6
Ill-Posedness	7
Restoration of Stability	8
Regularization and Discrepancy Principle	9
Fredholm Integral Equation	12
Phillips Solution	13
CHAPTER 3. INVERSE PROBLEMS IN ELECTROMAGNETICS	16
Differential Inverse Algorithms	16
Exact Methods	21
Integral Inverse Methods	23
Green's Function	23
Approximations of The Wave Equation	26
Born Approximation	26
Rytov Approximation	27
Resolving Power Theory	29
CHAPTER 4. NEURAL NETWORKS	33
Multi-Layer Perceptron	34

Back-Propagation Algorithm	36
Hopfield Networks	38
Stochastic Network	39
Deterministic Network	41
Linear Programming Network	49
CHAPTER 5. APPLICATION OF NEURAL NETWORKS FOR	
SOLVING INVERSE PROBLEMS	52
Solution of Inverse Problems Using the Perceptron	52
Results	53
Application: Flow Measurements	56
Solution of Inverse Problems Using Hopfield Network	59
Simulation of Energy Minimization	63
CHAPTER 6. INVERSE PROBLEM OF SCATTERING FROM	
LAYERED MEDIA	66
Horizontally Stratified Media	66
Forward Problem	67
Inverse Problem:	69
Radially Inhomogeneous Slab	72
Forward Problem	74
Inverse Problem	78
Summary of Algorithm	83
Simulation Results	84
CHAPTER 7. CONCLUSIONS	88

BIBLIOGRAPHY	91
ACKNOWLEDGEMENTS	97
APPENDIX A. GEOPHYSICS	99
Geophysical Surveying Methods	99
APPENDIX B. GROUNDWATER EXPLORATION	105

LIST OF FIGURES

Figure 3.1:	Two characteristic curves	19
Figure 4.1:	Multi-layer Perceptron	35
Figure 4.2:	Sigmoidal function	35
Figure 4.3:	Hopfield stochastic network	40
Figure 4.4:	Hopfield continuous network	42
Figure 4.5:	Neuron i	43
Figure 4.6:	Biological neural network	43
Figure 4.7:	Transfer function of amplifier	45
Figure 4.8:	Linear programming network	50
Figure 5.1:	True value for $z(x)$ and range of neural network solution for example 1	55
Figure 5.2:	Kernel $k(\xi)$ and input $u(\lambda)$ for example 2	56
Figure 5.3:	True value of $z(x)$ and range of neural network solution for example 2	57
Figure 5.4:	Ultrasonic measurement of flow	59
Figure 5.5:	Neural network with feedback circuit	63
Figure 6.1:	Horizontally stratified slab	67

Figure 6.2:	Coaxial cylinders model	73
Figure 6.3:	Transmission line analogy	76
Figure 6.4:	Transmission and reflection of Hankel and Bessel waves	76
Figure 6.5:	True distribution	85
Figure 6.6:	Initial value, 1st, and 2nd iterations	85
Figure 6.7:	3rd iteration	86
Figure 6.8:	Initial value, 1st, and 2nd iterations using amplitude of measurements	86
Figure 6.9:	3rd iteration using amplitude of measurements	87

CHAPTER 1. INTRODUCTION

Inverse problems are encountered in many fields of science and engineering. The inverse theory deals with the development of tools to extract useful information from physical measurements. The fitting of a curve to experimental data, as well as the problem of remote probing from satellite-borne systems, for example, involve the application of inverse theory.

Some of the fields where we encounter inverse problems are :

1. Medical tomography.
2. Plasma diagnostics.
3. Target recognition.
4. Earthquake location.
5. Analysis of molecular structure by X-ray diffraction.
6. Geophysics.
7. Recovering of defect shapes or profiles of material properties in the field of Non-destructive Evaluation (NDE).

Due to the complexities associated with inverse problem solutions, a lot of effort has been expended in the study of these problems. This thesis proposes a novel approach using neural networks for solving inverse problems.

Interest in neural networks historically has two roots [1] : (1) the desire to understand how a biological brain works, and (2) the wish to build machines that can perform cognitive tasks at which the human brain excels. Methods of achieving these objectives were the focus of intensive research in the field of *Artificial Intelligence* (AI).

In AI, a problem is solved by building an *Expert System*. This expert system consists of rule & knowledge data base, an inference engine, and an interface. The process of building the expert system begins by collecting information about the *reasoning* that governs the problem, whether it is formal information, from text books, or informal information, gained from experience. The reasoning is cast in the form of rules (IF – THEN statements) which are stored in the knowledge base. The inference engine is used to extract information from the knowledge base. If the user is not satisfied with the answer, he can interactively change the knowledge base using the interface.

Criticisms against AI include the fact that such approaches fail to simulate the operation of the human brain. First, in the area of natural language understanding, we cannot find all the rules governing the meaning of words and phrases, because they are context sensitive. Another area where AI approaches fail is in pattern recognition. Pattern recognition is a basic attribute of human brains as it is essential for recognizing and interacting with objects and persons. Criticism against AI techniques in the area of pattern recognition relates to the slowness of such methods. For example, when we recognize a person, our brains do not go through a process of searching through a large number of stored patterns of human faces to find the one that has the features closest to those of the person we see. This process will need a large

amount of time, particularly since the flow of signals in biological systems are 10 to 40 times slower than those of conventional computers. Human brains can retain and recall images without attempting to establish the geometrical relations between the objects contained in the image. This is in contrast to AI algorithms, where there is always a need to use rules.

Neural networks have emerged in recent years as an outcome of a desire to mimic the human brain. In AI we begin by reasoning and go *down* to decomposing the reasoning into rules. The neural networks approach on the contrary begins with a small building block, *the neuron*,. We then proceed to build a system by interconnecting a large number of neurons such that the output of the system matches the required solution to the problem. Early trials associated with building VLSI neural networks are reported in [1].

This thesis investigates a neural network approach for solving integral equations. We restrict our attention to the Fredholm integral equation of 1st kind which appears in many inverse problems. The primary advantage of the proposed method as compared to other computational methods is that it is potentially more stable. This is due to the parallel distributed processing structure of neural networks as well as the high degree of interconnectivity and feedback. Neural networks also offer the characteristics of generalization and error tolerance. A neural network with a large number of neurons will continue to function properly even in the case of failure of few neurons, whereas the performance of digital computers depends on the correctness of each bit of the data. The work described in the thesis consists of two parts.

In the first part a multilayer back-propagation network is trained using the input and output values of the integral equation. The network is then used to recover the

correct output when the input is corrupted with noise as is the case in practical field measurement systems.

The second part consists of the development of a Hopfield network for solving integral equations. The feasibility of the approach is demonstrated using an application in geophysics for reconstructing conductivity and/or permittivity values of a multilayered media from reflected wave measurements. Analysis of the method with regard to stability and convergence is presented.

Chapter 2 gives mathematical background of the general inverse problem. The ill-posedness of inverse problems, and the use of regularization technique for restoring stability of the solution are discussed. The development of the Fredholm integral equation for modeling inverse problems is presented. Chapter 3 first discusses the importance of electromagnetic fields in a wide range of applications. These applications include detecting and tracking targets using radar, remote sensing studies of the vegetation canopy, flaw detection and sizing in nondestructive evaluation (NDE), and in geophysical exploration for hydrocarbons, minerals, or groundwater. The mathematical analysis of electromagnetic inverse problems is then developed.

The topic of neural networks is discussed in chapter 4. Section 1 describes the multilayer perceptron, and the use of the back-propagation algorithm to train it. Section 2 discusses Hopfield neural networks. Digital stochastic networks, the continuous deterministic network, and linear programming networks are described. Analysis of the networks with regard to convergence and stability is presented.

Chapter 5 discusses the application of neural networks for solving inverse problems. Section 1 shows examples of solving inverse problems, described by integral equations, using multilayer perceptrons. An application of the algorithm, in the

field of flow measurements is discussed. Section 2 discusses the representation of inverse problems in the form of a function minimization problem, and the design of a Hopfield neural network for performing such minimizations. The use of Hopfield linear programming networks for finding the global minimum of the solution is also described.

Chapter 6 presents the application to two electromagnetic inverse problems in geophysics. Section 1 discusses the case of a horizontal transmitting loop over horizontally layered media. Section 2 discusses the use of loop transmitter, and receiver antennas in a borehole in axially symmetric media of complex permittivity. Simulation results are presented at the end of the chapter. Chapter 7 presents some concluding remarks.

Appendix A presents a brief introduction to conventional methods for solving inverse problems in geophysics. A specific example of an inverse problem as it relates to groundwater exploration is introduced in appendix B.

CHAPTER 2. INVERSE PROBLEMS

The terms “forward problem” and “inverse problem” are used to describe the performance of physical and engineering systems. In contrast to “forward problem”, where the system output is predicted from the model parameters, “inverse problem” involves the estimation of model parameters from the measured data. This can be summarized as follows:

Forward Problem:

model parameters \rightarrow model \rightarrow prediction of data

Inverse Problem:

data \rightarrow model \rightarrow estimation of model parameters

Mathematically [2] this can be formulated as follows:

Given:

- Z space of input quantities;
- U space of output quantities;
- IP space of system parameters;
- $A(p)$ system operator from U into Z ;
associated with $p \in IP$

The forward problem is defined as follows:

Given $z \in Z$ and $p \in IP$ find $u := A(p)z$

Inverse problems can be one of the following two types:

(a) reconstruction problem

Given $u \in U$ and $p \in IP$ solve the equation: $Az = u$ where $A := A(p)$

(b) identification problem

Given $u \in U$ and $z \in Z$ find $p \in IP$ such that:

$$A(p)z = u$$

The following sections describe the issue of stability associated with solutions of inverse problems and also methods for addressing these issues.

Ill-Posedness

In general, the solution to inverse problems is ill-posed. In [2], the definition of the term “ill-posed” is defined as follows:

For a problem represented by $Az = u$ ($z \in Z, u \in U$), the problem is well-posed in the sense of Hadamard, if the inverse map $A^{-1} : U \rightarrow Z$ exists, and is continuous; otherwise, the problem is ill-posed.

An example of an ill-posed problem is as follows:

Example:

Find $z=z(x,y)$ satisfying:

$$\frac{\partial^2 z}{\partial x^2} + \frac{\partial^2 z}{\partial y^2} = 0 \quad \text{in } \mathbb{R} \times (0, \infty)$$

$$z(x, 0) = 0, \quad \frac{\partial z}{\partial y}(x, 0) = u(x) \quad x \in \mathbb{R}$$

where $u(x) := U_n(x) := n^{-1} \sin(nx) \quad x \in \mathbb{R}, n \in \mathbb{N}, n \neq 0$

$$u_0(x) := 0$$

The solution is [2]:

$$z_n(x, y) = n^{-2} \sin(nx) \sinh(ny), \quad (x, y) \in \mathbb{R} \times (0, \infty) \quad n \in \mathbb{N}$$

$$z_0(x, y) = 0 \quad (x, y) \in \mathbb{R} \times (0, \infty)$$

We see that while u_n converges to u_0 , z_n does not converge to z_0 . In other words the solution for z does not depend continuously on data u , leading to instability of the solution process.

Restoration of Stability

As we have seen in the previous section, a major issue in the solution of the ill-posed inverse problems is the restoration of stability. This can be achieved by using a priori information about the problem. Tihonov [3] showed that the inverse mapping $U \rightarrow Z$ is stable if the class of admissible solutions is the compact class Z . This can be stated as: for every $\epsilon > 0$, there exists $\delta(\epsilon, Z)$ such that $\|u_1 - u_2\| < \delta$ implies $\|z_1 - z_2\| < \epsilon$. This can be expressed in the form of the following theorem [2]

Theorem 2.1 *Let U and Z be subsets of normalized spaces X and Y respectively, and let $A : Z \rightarrow U$ be a continuous mapping. If A is bijective (onto and one-to-one) and Z is compact, then $A^{-1} : U \rightarrow Z$ is continuous.*

The proof of the theorem can be shown by considering a sequence u_n in U with u as its limit. This corresponds in Z , to a sequence $z_n = A^{-1}(u_n)$, with $z = A^{-1}(u)$. Because Z is compact, a subsequence of z_n will converge to w in Z . From continuity of A , and the fact that A is injective (one-to-one), one can show that the image of w will be u , and $w = z$.

The problem now lies in ensuring that the space Z is compact. The solution proposed by Tihonov consists of regularization and is described below.

Regularization and Discrepancy Principle

Consider the system,

$$Az = u \quad (2.1)$$

For an element \bar{u} in U , and if $\bar{u} \in \mathcal{R}(A)$, where \mathcal{R} denotes range, there exists a unique $\bar{z} \in Z$. However, we can only compute a noisy estimate of \bar{u} , i.e., we can compute \tilde{u} such that:

$$\| \bar{u} - \tilde{u}_\epsilon \| \leq \epsilon < \| \tilde{u} \| \quad (2.2)$$

The second part of the above inequality implies that the signal to noise ratio is more than 1.

If A^{-1} is not bounded, the set of \tilde{z} will not be bounded, and we need a priori constraint expressed by:

$$\tilde{z} \in S$$

such that $A^{-1} : A(S) \rightarrow Z$ is a continuous mapping

A family of functions $z^\alpha(s)$ depending on a parameter α will be called [3] a *regularized* family of approximate solutions if:

- $u^\alpha(x) = A[x, z^\alpha(s)] \rightarrow \bar{u}(x)$ when $\alpha \rightarrow 0$
- For every α the functions $z^\alpha(s)$ belong to the compact class of functions \bar{Z} containing \bar{z}

The regularized family will converge uniformly to $\bar{z}(s)$ when $\alpha \rightarrow 0$. The solution to the regularization problem is achieved by minimizing a cost function M^α ,

$$M^\alpha[z(s), \bar{u}(x)] = N[z(s), \bar{u}(x)] + \alpha\Omega[z(s)]$$

where N is given by:

$$N[z(s), \bar{u}(x)] = \| A[x, z(s)] - \bar{u}(x) \|$$

and $\Omega[z(s)]$ is the regularizing functional chosen according to the application. Tikhonov chose Ω as follows:

$$\Omega[z(s)] = k(s) \| z'(s) \| + p(s) \| z(s) \| \quad (k > 0, p > 0)$$

Theorem 2.2 *For every function \bar{u} , there exists a unique continuous, differentiable function $z^\alpha(s)$ which makes the function $M^\alpha[z(s), \bar{u}(x)]$ a minimum.*

For proof see [3].

The choice of the regularization parameter $\alpha = \alpha(\epsilon)$ is decided such that for the measurements \tilde{u} , the solution z^α satisfies:

$$\| A\tilde{z}^\alpha - \tilde{u} \| = \epsilon \quad (2.3)$$

where ϵ is the noise level of the data. The left hand side of (2.3) is known as the discrepancy $D(\alpha, z^\alpha, \tilde{u})$, i.e.,

$$D(\alpha, z^\alpha, \tilde{u}) := \| Az^\alpha - \tilde{u} \| \quad (2.4)$$

Generally, there is a unique value for regularization parameter $\alpha = \alpha(\epsilon)$. In order to show the uniqueness of α , consider the problem,

$$Az = u \quad (2.5)$$

If we choose the solution z^α from the set C_ϵ ,

$$C_\epsilon = \{z : D(\alpha, z^\alpha, \tilde{u}) \leq \epsilon\} \quad (2.6)$$

such that z^α has the minimum norm, then the solution z^α will be unique and its corresponding discrepancy satisfies:

$$D(\alpha, z^\alpha, \tilde{u}) = \epsilon \quad (2.7)$$

If this is not the case, then from (2.6) we see that:

$$D(\alpha, z^\alpha, \tilde{u}) < \epsilon$$

and we can find a parameter $0 < t < 1$, such that as $t \rightarrow 1$, we have,

$$D(\alpha, tz^\alpha, \tilde{u}) < \epsilon$$

which implies that tz^α will have a smaller norm than z^α which contradicts the assumption that z^α has minimum norm. This discussion can be generalized by the following theorem[4]

Theorem 2.3 For u and \bar{u} satisfying (2.2), the function $\alpha \rightarrow D(\alpha, z, \bar{z})$ will be continuous, increasing and containing ϵ in its range

For proof see [4]

At this point we will illustrate the idea with a typical example of Fredholm integral equation, which is the focus of this thesis.

Fredholm Integral Equation

The Fredholm integral equation is encountered in different fields of applications. The equation can be written in the form:

$$h(x)z(x) + \int_a^b k(x, y)z(y)dy = u(x) \quad (c \leq x \leq d) \quad (2.8)$$

where: $u(x)$ denotes measured data

$k(x, y)$, the kernel function represents the conversion process.

$z(x)$, the required function that represents the system states .

If $h(x) \neq 0$ for $c \leq x \leq d$ the equation is of second kind.

If $h(x)=0$ the equation is said to be of first kind, as shown below.

$$\int_a^b k(x, y)z(y)dy = u(x) \quad (c \leq x \leq d) \quad (2.9)$$

Several problems arise when trying to solve a Fredholm integral equation of the first kind, for a given data $u(x)$, even with modest accuracy. The reason for this is inherent in the equation itself. For example [4, 5], for any square integrable $k(.,.)$, we have

$$\int_0^\pi k(x, y) \sin(my)dy \rightarrow u_m \quad (2.10)$$

where

$$u_m \rightarrow 0 \text{ as } m \rightarrow \infty$$

From equation (2.9), if we add ($z_m = \sin my$) to $z(y)$ then:

$$\int_0^\pi k(x, y)(z(x) + A \sin(my)) dy \rightarrow u(x) \text{ as } m \rightarrow \infty$$

For large values of m , the measured data $\tilde{u}(x)$,

$$\begin{aligned} \tilde{u}(x) &= u(x) + u_m \\ &= A \int_0^\pi k(x, y) \sin(my) dy \end{aligned}$$

will correspond to a solution $z(x) + z_m$ where $z_m := A \sin my$

Hence, even an infinitesimal change u_m in u would cause finite change z_m in z , i.e., the equation is unstable. Also, $u_m \rightarrow 0$ as $m \rightarrow \infty$ faster for flat smooth kernels than for sharply peaked kernels. Hence, the success in solving (2.9) depends to a large extent on the accuracy of $u(x)$ and the shape of $k(x, y)$.

Phillips Solution

Phillips [5] suggested a method for solving the linear equation of the first kind, of the form:

$$\int_a^b k(x, y)f(y)dy = g(x) + \epsilon(x) \quad (a \leq x \leq b) \quad (2.11)$$

where $\epsilon(x)$ represents the truncation error in $g(x)$.

In general equation (2.11) is satisfied by a family \mathcal{F} of solutions. In order to obtain the unique solution f from \mathcal{F} , Phillips imposed the constraint of smoothness,

i.e. $f = f_s \in \mathcal{F}$ such that f_s is the smoothest in some sense. This constraint can be expressed as

$$\int_a^b (f_s'')^2 dx = \min_{f \in \mathcal{F}} \int_a^b (f'')^2 dx \quad (2.12)$$

Equations (2.11) and (2.12) are solved numerically. From (2.11) we obtain:

$$\sum_{i=0}^n w_i k_{ji} f_i = g_j + \epsilon_j \quad (j = 0, 1, \dots, n) \quad (2.13)$$

which can be written in matrix form as:

$$A \underline{f} = \underline{g} + \underline{\epsilon} \quad (2.14)$$

From (2.12) we get:

$$\sum_{i=0}^n (f_{i+1}^s - 2f_i^s + f_{i-1}^s)^2 = \min_{f \in \mathcal{F}} \sum_{i=0}^n (f_{i+1} - 2f_i + f_{i-1})^2 \quad (2.15)$$

f_s can be cast as the vector that minimizes :

$$\lambda \sum_{i=0}^n (f_{i+1} - 2f_i + f_{i-1})^2 + \sum_{i=0}^n \epsilon_i^2 \quad (2.16)$$

where λ is a positive constant referred to as the Lagrange multiplier. Equation (2.16) can be written in the form:

$$\lambda B \underline{f}_s + \underline{\epsilon} = 0 \quad (2.17)$$

where,

$$B_{lk} = \alpha_{k-2,l} - 4\alpha_{k-1,l} + 6\alpha_{k,l} - 4\alpha_{k+1,l} + \alpha_{k+2,l} \quad (k, l = 0, 1, \dots, n)$$

and, $\alpha_{ij} = \frac{\partial f_i}{\partial \epsilon_j}$ ($i, j = 0, 1, \dots, n$)

For $\lambda = 0$

$$A \underline{f} = \underline{g}$$

For $\lambda \neq 0$, we have equation (2.14). From (2.14), and (2.17), we get:

$$\epsilon = -\lambda B f_s \quad (2.18)$$

$$f_s = (A + \lambda B)^{-1} g \quad (2.19)$$

CHAPTER 3. INVERSE PROBLEMS IN ELECTROMAGNETICS

Electromagnetic methods are frequently used in a variety of applications ranging from medical diagnosis to geophysics. This is largely due to the fact that in electromagnetic methods, there is no need for physical contact of measuring transducer with the system, and thus measurements can be taken easily, even from satellites or aircraft. Different measurements can be taken by only changing the frequency of operation without the need for changing the experimental setup. We will discuss here some of the analytical methods that are used in solving inverse problems in electromagnetics.

Differential Inverse Algorithms

These methods are based on the differential equations governing the fields. Two of these methods were discussed in [6] , and [7] namely *Cholesky method* and *the method of characteristics*. We will limit our discussion to the latter algorithm.

We start with Maxwell's equations:

$$\nabla \times \underline{E} = -\mu \frac{\partial \underline{H}}{\partial t} \quad (3.1)$$

$$\nabla \times \underline{H} = \epsilon_0 \epsilon_c \frac{\partial \underline{E}}{\partial t} \quad (3.2)$$

where complex permittivity ϵ_c is given as:

$$\epsilon_c = \epsilon' + j\epsilon'' = \left(\frac{\epsilon}{\epsilon_0} + j \frac{\sigma}{\omega\epsilon_0} \right)$$

Taking the curl of (3.1) and substituting with (3.2), we get

$$\nabla^2 \underline{E} = \mu \frac{\partial}{\partial t} \left\{ \left(\epsilon + j \frac{\sigma}{\omega} \right) \frac{\partial \underline{E}}{\partial t} \right\} \quad (3.3)$$

If we consider a steady state solution with $\underline{E} = \underline{E}e^{-j\omega t}$, i.e. $\frac{\partial}{\partial t} = -j\omega$, we get

$$\nabla^2 \underline{E} = \mu\epsilon \frac{\partial^2 \underline{E}}{\partial t^2} + \mu\sigma \frac{\partial \underline{E}}{\partial t} \quad (3.4)$$

Consider the special case of infinite source from $y = -\infty$ to $y = \infty$ at $z = z_m$. In this case the non-vanishing components are E_y, H_x , and H_z . Consider also the case where μ is equal to μ_0 . From (3.4) we get:

$$\frac{\partial^2 E_y}{\partial x^2} + \frac{\partial^2 E_y}{\partial z^2} - \frac{1}{c^2} \frac{\partial^2 E_y}{\partial t^2} - \frac{1}{c^2 T(z)} \frac{\partial E_y}{\partial t} = 0 \quad (3.5)$$

where, $c(z) = \frac{1}{\sqrt{\mu_0\epsilon(z)}}$, and $T(z) = \frac{\epsilon(z)}{\sigma(z)}$, with the boundary conditions:

$$E_y(x, z_m, t) = e(x, t) \quad (3.6)$$

$$(3.7)$$

$$\begin{aligned} \frac{\partial E_y}{\partial z} &= \mu_0 \frac{\partial H_x}{\partial t}(x, z_m, t) \\ &= \mu_0 \frac{\partial}{\partial t} h(x, t) \end{aligned} \quad (3.8)$$

where, $e(x,t)$ and $h(x,t)$ are measured values.

Let $u(k_x, z, t)$ be a weighted Fourier transform of $E_y(x, z, t)$, s.t.,

$$\begin{aligned} E_y(x, z, t) &= \int_{-\infty}^{\infty} dk_x e^{ik_x x} e^{|k_x|(z-z_m)} u(k_x, z, t) \\ &= \mathcal{F}^{-1} \{u(k_x, z, t)\} \end{aligned} \quad (3.9)$$

Therefore:

$$\frac{\partial^2 E_y}{\partial x^2} = -k_x^2 E_y \quad (3.10a)$$

$$\frac{\partial E_y}{\partial z} = |k_x| E_y + \mathcal{F}^{-1}\{u_z\} \quad (3.10b)$$

$$\frac{\partial^2 E_y}{\partial z^2} = k_x^2 E_y + 2|k_x| \mathcal{F}^{-1}\{u_z\} + \mathcal{F}^{-1}\{u_{zz}\} \quad (3.10c)$$

Substituting (3.10a)-(3.10c) into (3.5), we get:

$$2|k_x| \mathcal{F}^{-1}\{u_z\} + \mathcal{F}^{-1}\{u_{zz}\} - \frac{1}{c^2} \frac{\partial^2 E_y}{\partial t^2} - \frac{1}{c^2 T} \frac{\partial E_y}{\partial t} = 0 \quad (3.11)$$

The Fourier transform of (3.11) gives

$$u_{zz} - \frac{1}{c^2} u_{tt} + 2|k_x| u_z - \frac{1}{c^2 T} u_t = 0 \quad (3.12a)$$

with boundary conditions

$$u_t(k_x, z_m, t) = \mathcal{F}\{e_t(x, t)\} \quad (3.12b)$$

$$u_z(k_x, z_m, t) = \mu_0 \mathcal{F}\{h(x, t)\} - |k_x| \mathcal{F}\{e(x, t)\} \quad (3.12c)$$

Defining travel time τ

$$\tau = \int_{z_m}^z \frac{dz'}{c(z')} \quad z \geq z_m \quad (3.13)$$

we get

$$\frac{d\tau}{dz} = \frac{1}{c(z)} \quad (3.14a)$$

$$u_z = u_\tau \frac{1}{c(z)} \quad (\text{chain rule}) \quad (3.14b)$$

$$u_{zz} = \frac{u_{\tau\tau}}{c^2} - \frac{u_\tau}{c} c_\tau \quad (3.14c)$$

From (3.12a)-(3.12c) and (3.14a)-(3.14c) we get

$$u_{\tau\tau} - u_{tt} + (2|k_x|c - \frac{c_\tau}{c})u_\tau - \frac{1}{T}u_t = 0 \quad (3.15a)$$

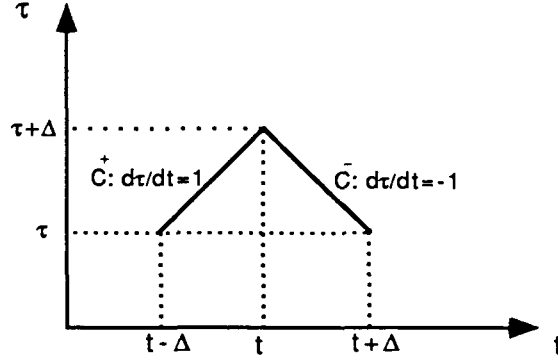


Figure 3.1: Two characteristic curves

with boundary conditions

$$u_t(k_x, \tau = 0, t) = \mathcal{F}\{e_t(x, t)\} \quad (3.15b)$$

$$u_\tau(k_x, \tau = 0, t) = c(0) [\mu_0 \mathcal{F}\{h_t(x, t)\} - |k_x| \mathcal{F}\{e_t(x, t)\}] \quad (3.15c)$$

. In [8], for an equation of the form :

$$Au_{\tau\tau} + Bu_{\tau t} + Cu_{tt} = D \quad (3.16)$$

where A, B, C, τ are functions of u, τ, t, u_t, u_τ , we have for the characteristic curves

$$\left(\frac{d\tau}{dt}\right)_{char} = \frac{B \pm \sqrt{B^2 - 4AC}}{2A} \quad (3.17)$$

For equation (3.15a) where $B = 0$, $A = 1$, and $C = -1$, we get, (Figure 3.1)

$$C^\pm := \left(\frac{d\tau}{dt}\right)_{char} = \pm 1 \quad (3.18)$$

We express (3.15a) in terms of derivatives du_τ , du_t , on the characteristic curves given in (3.18), where

$$du = \frac{\partial u}{\partial \tau} d\tau + \frac{\partial u}{\partial t} dt$$

on C^\pm :

$$\begin{aligned} du &= d\tau \left\{ \frac{\partial u}{\partial \tau} \pm \frac{\partial u}{\partial t} \right\} \\ du_\tau &= \{u_{\tau\tau} \pm u_{\tau t}\} d\tau \\ du_t &= \{u_{t\tau} \pm u_{tt}\} d\tau \end{aligned}$$

Substituting in (3.15a), we get:

$$du_\tau \mp du_t + \left[\{2|k_x|c - \frac{c_\tau}{c}\} u_\tau - \frac{1}{T} u_t \right] d\tau = 0 \quad \text{on } C^\pm \quad (3.19)$$

This can be written in difference form as:

$$\begin{aligned} u_\tau(\tau + \Delta, t) - u_\tau(\tau, t \mp \Delta) \mp [u_t(\tau + \Delta, t) - u_t(\tau, t \mp \Delta)] \\ + 2 \left[\left\{ |k_x|c(\tau) - \frac{c_\tau(\tau)}{c(\tau)} \right\} - \frac{1}{T} u_t(\tau, t \mp \Delta) \right] \Delta = 0 \end{aligned}$$

Therefore,

$$\begin{aligned} \begin{bmatrix} u_\tau(\tau + \Delta, t) \\ u_t(\tau + \Delta, t) \end{bmatrix} &= \frac{1}{2} \begin{bmatrix} A_{11} & A_{12} \\ A_{21} & A_2 \end{bmatrix} \begin{bmatrix} u_\tau(\tau, t + \Delta) \\ u_t(\tau, t + \Delta) \end{bmatrix} \\ &+ \frac{1}{2} \begin{bmatrix} B_{11} & B_{12} \\ B_{21} & B_2 \end{bmatrix} \begin{bmatrix} u_\tau(\tau, t - \Delta) \\ u_t(\tau, t - \Delta) \end{bmatrix} \end{aligned} \quad (3.20)$$

where:

$$A_{11} = A_{21} = B_{11} = -B_{21} = 1 - \{2|k_x|c(\tau) - r(\tau)\} \Delta$$

$$A_{12} = A_{22} = 1 + \frac{\Delta}{T(\tau)}$$

$$r(\tau) = \frac{c_\tau(\tau)}{c(\tau)}$$

For causality we have

$$u(\tau, t) = 0 \quad \text{for } t \leq \tau$$

If we let $t = \tau + \Delta$ in (3.20), we get:

$$A \begin{bmatrix} u_\tau(\tau, \tau + 2\Delta) \\ u_t(\tau, \tau + 2\Delta) \end{bmatrix} = 0$$

Therefore:

$$A_{11}u_\tau(\tau, \tau + 2\Delta) + A_{12}u_t(\tau, \tau + 2\Delta) = 0 \quad (3.21)$$

Substituting

$$c_\tau(\tau) \approx \frac{1}{\Delta}[c(\tau + \Delta) - c(\tau)]$$

equation (3.21) can be written as:

$$c(\tau + \Delta) = c(\tau) \left[2|k_x|c(\tau)\Delta - \left(1 + \frac{\Delta}{T(\tau)} \right) \frac{u_t(\tau, \tau + 2\Delta)}{u_\tau(\tau, \tau + 2\Delta)} \right] \quad (3.22)$$

Equation (3.22) is used to propagate solutions for $c(\tau)$, $T(\tau)$ from boundary conditions values [8].

Exact Methods

Exact methods belong to the class of strategies where the approach is to compute approximately a function which exactly solves the inverse problem. In many cases, the approximation arises due to the digital representation of differentiation and integration operators. Gel'fand and Levitan proposed these methods in 1951. Exact methods were applied for inferring the accoustical impedance of a horizontally layered medium [9]. The application of the method in electromagnetic inversion problems is found in [6], [10], and [11].

Maxwell's equations for electromagnetic wave propagation along the z -axis, normal to a slab of permittivity $\epsilon(z)$ and conductivity $\sigma(z)$ reduces to the following

equation.

$$E_{zz} - \epsilon(z)\mu_0 E_{tt} - \sigma(z)\mu_0 E_t = 0$$

which is a differential equation of the form

$$u_{xx} - u_{tt} + A(x)u_x + B(x)u_t + C(x)u = 0$$

with $C(x) = 0$

We want to solve for the coefficients of the differential equation.

In [7], a Schrödinger wave equation is obtained from this differential equation for the lossless case using the transform:

$$\frac{d\tau}{dz} = \frac{1}{c}$$

Then, normalizing $E(\tau, t)$ & $H(\tau, t)$ by:

$$e(\tau, t) = \frac{1}{\sqrt{\eta}} E(\tau, t)$$

$$h(\tau, t) = \sqrt{\eta} H(\tau, t)$$

where: $\eta = \mu_0 c(\tau)$, we get:

$$e_{\tau\tau} - e_{tt} - V e = 0 \quad (\text{Schrödinger equation})$$

where $V = \frac{q_{\tau\tau}}{q}$, $q = [c(\tau)]^{-1/2}$

As explained in [11] we can get V from knowledge of the scattering kernels R_{\pm}, T_{\pm} which we get directly from measurements using waves which closely approximate a delta function.

Integral Inverse Methods

In integral inverse methods, we represent field quantities in the integral equation in terms of the source and Green's function. Solutions are obtained by iterative solution of the integral equation.

Green's Function

Consider a wave equation of the form:

$$(\nabla^2 + k^2)f(\underline{r}) = d(\underline{r}) \quad (3.23)$$

where $d(\underline{r})$ represents the source, and $f(\underline{r})$ represents the field. The Green's function represents the field $f(\underline{r})$ due to a δ function source at \underline{r}' .

$$(\nabla^2 + k^2)G(\underline{r}, \underline{r}') = -\delta(\underline{r} - \underline{r}') \quad (3.24)$$

The solution of the wave equation is :

$$f(\underline{r}) = \int_{vol.} d(\underline{r}')G(\underline{r}, \underline{r}')dv' \quad (3.25)$$

Following discussions in [12] , we can obtain Green's function as follows:

Considering the triple Fourier transform:

$$\tilde{\tilde{F}}(\underline{\alpha}) = (2\pi)^{-\frac{3}{2}} \int_{-\infty}^{\infty} \int_{-\infty}^{\infty} \int_{-\infty}^{\infty} F(\underline{r}) \exp(-j\underline{\alpha} \cdot \underline{r}) d\underline{r}$$

$$F(\underline{r}) = (2\pi)^{-\frac{3}{2}} \int_{-\infty}^{\infty} \int_{-\infty}^{\infty} \int_{-\infty}^{\infty} \tilde{\tilde{F}}(\underline{\alpha}) \exp(j\underline{\alpha} \cdot \underline{r}) d\underline{\alpha}$$

$$\underline{\alpha} = \alpha_1 \hat{\alpha}_1 + \alpha_2 \hat{\alpha}_2 + \alpha_3 \hat{\alpha}_3$$

$$d\underline{r} = dx dy dz$$

$$d\alpha = d\alpha_1 d\alpha_2 d\alpha_3$$

Applying triple Fourier transform to (3.24), we get:

$$\text{Right hand side} = -(2\pi)^{-\frac{3}{2}} \exp(-\alpha \cdot \underline{r}')$$

On the left hand side, we have the integral:

$$\mathcal{I} = \int_{-\infty}^{\infty} \exp(-j\alpha_v x_v) \frac{\partial^2 G}{\partial x_v^2} dx_v \quad (v = 1 \dots 3)$$

Using Integration by parts, we get \mathcal{I} as :

$$\mathcal{I} = \left[\exp(-j\alpha_v x_v) \left(\frac{\partial G}{\partial x_v} + j\alpha_v G \right) \right]_{-\infty}^{\infty} - \alpha^2 \int_{-\infty}^{\infty} G e^{-j\alpha x_v} dx_v \quad (3.26)$$

If the first term of right hand side of (3.26) equals zero, we can see that the Fourier transform of $\nabla^2 G$ is given by $-\alpha^2 \tilde{\tilde{G}}(\alpha)$.

Therefore,

$$\begin{aligned} -\alpha^2 \tilde{\tilde{G}}(\alpha) + k^2 \tilde{\tilde{G}}(\alpha) &= -(2\pi)^{-3/2} \exp(-j\alpha \cdot \underline{r}) \\ \tilde{\tilde{G}}(\alpha) &= (2\pi)^{-3/2} \frac{\exp(-j\alpha \cdot \underline{r})}{\alpha^2 - k^2} \end{aligned}$$

Taking the inverse Fourier transform of the above equation, we get:

$$\begin{aligned} G(\underline{r}, \underline{r}') &= (2\pi)^{-3} \iiint \frac{\exp(j\alpha \cdot (\underline{r} - \underline{r}'))}{\alpha^2 - k^2} d\alpha \\ &= (2\pi)^{-3} \iiint \frac{\exp(j\alpha R \cos \theta)}{\alpha^2 - k^2} d\alpha \end{aligned}$$

where, $\underline{R} = \underline{r} - \underline{r}'$, and θ is the angle between vectors $\underline{\alpha}$ and \underline{R} . If we rotate the axes so that \underline{R} lies on α_3 , we get:

$$G(\underline{r}, \underline{r}') = (2\pi)^{-3} \int_{\alpha=0}^{\infty} \int_{\theta=0}^{\pi} \int_{\phi=0}^{2\pi} \frac{\exp(j\alpha R \cos \theta)}{\alpha^2 - k^2} \alpha^2 d\alpha \sin \theta d\theta d\phi$$

$$\begin{aligned}
&= \frac{1}{(4\pi^2 R)} \int_{-\infty}^{\infty} \frac{\sin(\alpha R)}{\alpha^2 - k^2} \alpha d\alpha \\
&= \frac{-j}{8\pi^2 R} \left[\int_{-\infty}^{\infty} \frac{e^{j\beta} \beta d\beta}{(\beta + \gamma)(\beta - \gamma)} - \int_{-\infty}^{\infty} \frac{e^{-j\beta} \beta d\beta}{(\beta + \gamma)(\beta - \gamma)} \right]
\end{aligned}$$

where $\beta = \alpha R$ and $\gamma = kR$

Integrating in the complex domain using the residue theorem, we get:

$$G(\underline{r}, \underline{r}') = \frac{e^{jkR}}{4\pi R} \quad (3.27)$$

Note that substituting G given in (3.27) into (3.26) assures that the 1st term in right hand side is zero.

In the axisymmetric case the wave equation is modified to :

$$(\nabla_{xy}^2 + k^2)G(\rho, \rho') = -\delta(\rho - \rho')$$

Applying the same procedure as was used for the three-dimensional case, and using two-dimensional Fourier transform, we get:

$$\begin{aligned}
G(\rho, \rho') &= (2\pi)^{-2} \int_{-\infty}^{\infty} \int_{-\infty}^{\infty} \frac{\exp(j\underline{\alpha} \cdot (\underline{\rho} - \underline{\rho}'))}{\alpha^2 - k^2} d\underline{\alpha} \\
\underline{\alpha} &= \alpha_1 \hat{\alpha}_1 + \alpha_2 \hat{\alpha}_2
\end{aligned} \quad (3.28)$$

Using the substitution $\alpha_1 = \lambda \cos \beta$ and $\alpha_2 = \lambda \sin \beta$, we get:

$$G(\underline{\rho}, \underline{\rho}') = (2\pi)^{-2} \int_{-\infty}^{\infty} \frac{\lambda d\lambda}{\lambda^2 - k^2} \int_{-\pi}^{\pi} \exp(j\lambda |\underline{\rho} - \underline{\rho}'| \cos(\beta - \phi)) d\beta \quad (3.29)$$

where ϕ is the angle between $\underline{\alpha}$ and $(\underline{\rho} - \underline{\rho}')$. Equation (3.29) can be written in the form:

$$G(\underline{\rho}, \underline{\rho}') = (4\pi)^{-1} \int_{-\infty}^{\infty} \frac{H_0^{(1)}(\lambda |\underline{\rho} - \underline{\rho}'|)}{\lambda^2 - k^2} \lambda d\lambda$$

where $H_0^{(1)}$ is Hankel function of first kind and zero order. The integration can be performed in the complex plane . The integral is equal to $(2\pi j (\text{Residue at the pole } \lambda = k))$

$$G(\rho, \rho') = \frac{j}{4} H_0^{(1)}(k|\rho - \rho'|)$$

Approximations of The Wave Equation

Born Approximation

For source free region equation (3.23) can be written in the form

$$(\nabla^2 + k_0^2)f(\underline{r}) = -O(\underline{r})f(\underline{r}) \quad (3.30)$$

where k_0 is the wave number in free space and $O(\underline{r})$ is given by:

$$O(\underline{r}) = k^2 - k_0^2$$

The field $f(\underline{r})$ can be represented by two components

$$f(\underline{r}) = f_0(\underline{r}) + f_s(\underline{r}) \quad (3.31)$$

where $f_0(\underline{r})$ is the solution in free space, i.e.,

$$(\nabla^2 + k_0^2)f_0(\underline{r}) = 0 \quad (3.32)$$

Substituting (3.31) and (3.32) in (3.30) we get

$$(\nabla^2 + k_0^2)f_s(\underline{r}) = -O(\underline{r})f(\underline{r}) \quad (3.33)$$

Therefore,

$$f_s(\underline{r}) = \int G(\underline{r} - \underline{r}')O(\underline{r}')f(\underline{r}')d\underline{r}' \quad (3.34)$$

Equation (3.34) is exact, but the problem is that $f(\underline{r})$ in the left hand side is a function of incident and scattered fields. *The first Born approximation* is to let $f(\underline{r}) = f_0(\underline{r})$ in the integral. A more accurate solution is obtained by using an iterative algorithm where $f(\underline{r})$ is represented as

$$f(\underline{r}) = f_0(\underline{r}) + f_1(\underline{r}) + f_2(\underline{r}) + \dots$$

where,

$$f_{i+1}(\underline{r}) = \int f_i(\underline{r}') O(\underline{r}) G(\underline{r} - \underline{r}') d\underline{r}'$$

Rytov Approximation

Another approximation used to get the scattered field is Rytov approximation [13].

Representing the field as a complex phase

$$f(\underline{r}) = e^{\phi(\underline{r})}$$

We get in a source free region

$$(\nabla^2 + k^2)e^{\phi} = 0$$

Therefore,

$$\begin{aligned} \nabla \cdot (e^{\phi} \nabla \phi) + k^2 e^{\phi} &= 0 \\ e^{\phi} \nabla^2 \phi + (\nabla \phi)^2 e^{\phi} + k_0^2 e^{\phi} &= -O(\underline{r}) \end{aligned} \quad (3.35)$$

If we write $\phi(\underline{r}) = \phi_0(\underline{r}) + \phi_s(\underline{r})$, where $e^{\phi_0(\underline{r})} = f_0(\underline{r})$, and substituting in (3.35) we get,

$$\begin{aligned} (\nabla \phi_0)^2 + 2\nabla \phi_0 \cdot \nabla \phi_s + (\nabla \phi_s)^2 + \\ + \nabla^2 \phi_0 + \nabla^2 \phi_s + k_0^2 + O(\underline{r}) &= 0 \end{aligned} \quad (3.36)$$

Knowing that ϕ_0 satisfies equation (3.35), with $O(r) = 0$ i.e.,

$$\nabla^2 \phi_0 + (\nabla \phi_0)^2 + k_0 = 0$$

Equation (3.36) becomes:

$$2\nabla \phi_0 \cdot \nabla \phi_s + \nabla^2 \phi_s = -(\nabla \phi_s)^2 - O(r) \quad (3.37)$$

The left hand side in (3.37) can be expressed in another form by the following substitution steps:

$$\begin{aligned} \nabla^2(f_0 \phi_s) &= \nabla \cdot \nabla(f_0 \phi_s) \\ &= \nabla \cdot (f_0 \nabla \phi_s + \phi_s \nabla f_0) \\ &= f_0 \nabla^2 \phi_s + 2\nabla f_0 \cdot \nabla \phi_s + \phi_s \nabla^2 f_0 \end{aligned} \quad (3.38)$$

In (3.38) we use the substitutions :

$$\nabla^2 f_0 = -k_0^2 f_0$$

and

$$\begin{aligned} \nabla f_0 &= \nabla e^{\phi_0} \\ &= e^{\phi_0} \nabla \phi_0 \\ &= f_0 \nabla \phi_0 \end{aligned}$$

Equation (3.38) becomes:

$$2f_0 \nabla \phi_0 \cdot \nabla \phi_s + f_0 \nabla^2 \phi_s = \nabla^2(f_0 \phi_s) + k_0^2 f_0 \phi_s \quad (3.39)$$

Substituting (3.39) in (3.37) we get

$$(\nabla^2 + k_0^2)(f_0 \phi_s) = -f_0 [(\nabla \phi_s)^2 + O(r)]$$

Therefore,

$$f_0 \phi_s = \int_{v'} G(\underline{r} - \underline{r}') f_0(\underline{r}') [(\nabla \phi_s)^2 + O(\underline{r})] d\underline{r}' \quad (3.40)$$

If we neglect $(\nabla \phi_s)^2$ with respect to $O(\underline{r})$ we get

$$f_0 \phi_s = \int_{v'} G(\underline{r} - \underline{r}') f_0(\underline{r}') O(\underline{r}) d\underline{r}' \quad (3.41)$$

Therefore, $\phi_s = \frac{f_B(\underline{r})}{f_0(\underline{r})}$, where $f_B(\underline{r})$ is Born approximation of the field.

Resolving Power Theory

This theory was introduced by Backus-Gilbert[14, 15], as they investigated the internal structure of the earth from seismic data. Parker [16, 17] applied the method for estimating the conductivity profiles in the mantle. Fullagar et al [18] used the method to invert frequency sounding for data relating to a horizontal loop antenna. Coen[19], and Coen et al [20] used the method to assess the reliability of estimates and to compute the resolution of the estimates using a quasi-Newton iterative scheme.

To understand the theory, we consider the discrete case explained in [21]. Let the system be described by:

$$G \underline{m} = \underline{d}$$

where: G is the $M \times N$ kernel matrix.

\underline{m} is the $N \times 1$ system parameter vector.

\underline{d} is the $M \times 1$ measured data vector.

In general, the estimated value of \underline{m} can be written in the form:

$$\underline{m}^{est} = G^{-g} \underline{d}^{obs}$$

where: G^{-g} is the generalized inverse of G .

d^{obs} is the observed data.

$$\begin{aligned} \therefore \underline{m}^{est} &= G^{-g} [G \underline{m}^{true}] \\ &= G^{-g} G \underline{m}^{true} \\ &= R \underline{m}^{true} \end{aligned}$$

The matrix R ($M \times M$) is called *the Resolution Matrix*. If $R = I$ (identity matrix), then each model parameter is uniquely determined; otherwise, each element of \underline{m}^{est} is a linear combination of some or all elements of \underline{m}^{true} .

We can also define *Data Resolution Matrix* N , where \underline{d}^{pre} , the predicted values of \underline{d} , is related to N as follows:

$$\begin{aligned} \underline{d}^{pre} &= G \underline{m}^{est} \\ &= G G^{-g} \underline{d}^{obs} \\ &= N \underline{d}^{obs} \end{aligned}$$

A measure of goodness of R , and N matrices can be taken as the norm of difference between resolution matrix and identity matrix I . This is known as *Dirichlet spread* of resolution matrix. The problems encountered may be over-determined, or under-determined. For over-determined problems, we can choose the least square error solution and R can become equal to I . However, for under-determined problems, other constraints have to be added to the problem. For instance, to obtain a solution that minimizes the L_1 or L_2 norm, or to get the smoothest solution, the resolution matrix R will not be an identity matrix. It can be shown that L_2 norm solution results in the minimization of Dirichlet spread of R .

Backus-Gilbert method considers the case of natural order of data, and therefore, choice of spread gives more weight to nearby data. For example, a natural order of data is found in the geophysical problem where \underline{d} represents a function of conductivity σ at different depths.

$$d_i = d_i(\sigma)$$

$$d_i^{obs} = d_i(\sigma^{true})$$

Fundamental to this scheme are the Fréchet kernels $\{F_i(z): i=1 \dots N\}$ used for expressing small changes in the observed data corresponding to a small change $\delta\sigma(z)$ in σ .

$$\delta d_i^{obs} = \int_0^{\infty} F_i(z) \delta\sigma(z) dz + O \|\delta\sigma\|^2 \quad (3.42)$$

where: $O \|\delta\sigma\|^2 \rightarrow 0$ faster than $\|\delta\sigma\|$. If (3.42) holds, the data are said to be Fréchet-differentiable.

An average value $\langle \sigma(z_0) \rangle$ is defined by Backus-Gilbert(1968) as the inner product of an acceptable $\sigma(z)$ with resolution function $R(z, z_0)$, [18].

$$\langle \sigma(z_0) \rangle = \int_0^{\infty} R(z, z_0) \sigma(z) dz \quad (3.43)$$

where the averaging function (or the resolution window) is a linear combination of Fréchet kernels, i.e.,

$$R(z, z_0) = \sum_{i=1}^N a_i(z_0) F_i(z) \quad (3.44)$$

If $\sigma_1(z)$ and $\sigma_2(z)$ are distinct acceptable conductivities, then:

$$\langle \sigma_1(z) \rangle = \langle \sigma_2(z) \rangle + O \|\sigma_1 - \sigma_2\|^2$$

The coefficients $a_i(z_0)$ are chosen to minimize the spread $S(z_0)$ defined by Backus and Gilbert (1970) as:

$$S(z_0) = 12 \int_0^{\infty} (z - z_0)^2 R^2(z, z_0) dz \quad (3.45)$$

such that $\int_0^{\infty} R(z, z_0) dz = 1$

The factor $(z - z_0)^2$ reflects the natural order of data giving more weight to nearby data points. Minimizing the spread will give rise to larger variance of the average function , i.e., there is a *trade-off* between spread and variance.

CHAPTER 4. NEURAL NETWORKS

Interest in neural networks within the engineering community is not recent. It can be traced back to the early 1940s to the work of McCullugh and Pitts [22]. Some work on neural networks was done by few research groups by 1960s. The two most active research groups were those of Widrow at Stanford, and Rosenblatt at Cornell [23]. Widrow developed the first hardware implementation of neural networks with the introduction of the adaptive linear element, or the adaline. Rosenblatt introduced the single layer perceptron and the multilayer perceptron. However, interest in neural networks was reduced in the 1970s due to the lack of development of learning rules for adjusting the weights between the neurons. One of the first learning rules was due to Hebb presented in 1957. Here the underlying philosophy is that of *unsupervised* learning, where the learning does not depend on reference data. Supervised learning rules were then developed, and the backpropagation algorithm vitalized multilayer perceptrons [24]. This led the dramatic return of neural networks in the 1980s.

Basically, artificial neural networks attempt to mimic the biological neural systems with respect to both the neural architectures as well as information processing strategies. A simplification of a biological neuron is shown in [24]. A biological neuron consists of a soma, dendrites, and axons. The dendrite brings the input signals to the neuron, and the axon carries the output. The axons are connected to dendrites of

other cells through synapses. In the soma, a summation of input signals is computed, and the neuron will fire if the sum is larger than a threshold. A human brain has approximately 10^{11} neurons and 10^{14} synapses.

There are different classes of artificial neural networks based on different network architecture and neuron characteristics such as neuron transfer functions and threshold values. Neural networks can also differ in the training rules applied for adjusting the weights of synapses. Lippmann [25] has represented a review of different types of artificial neural networks. We present here two kinds of artificial neural networks, the multilayer perceptron, and Hopfield networks, which are used in inverse problem solutions.

Multi-Layer Perceptron

Multi-layer perceptrons, (Figure 4.1) are feed-forward nets with one or more layers of nodes, known as hidden layers, that lie between the input layer and output layer. The nodes of the network are non-linear elements, and their transfer function is usually chosen to be a sigmoidal function as shown in Figure 4.2.

The perceptron is commonly used in pattern recognition applications. For a certain input vector applied to the perceptron, the output specifies the cluster that includes this vector. The net is first trained by applying some known pairs of input-output vectors to the network. This is known as the training phase. During training, the weights are adjusted so that correct output emerges for input vectors in the training data. The network is then used for computing the output for test data not used in the training phase. For example an application of the multilayer perceptron for pattern recognition in the field of nondestructive evaluation is presented in [26]. The

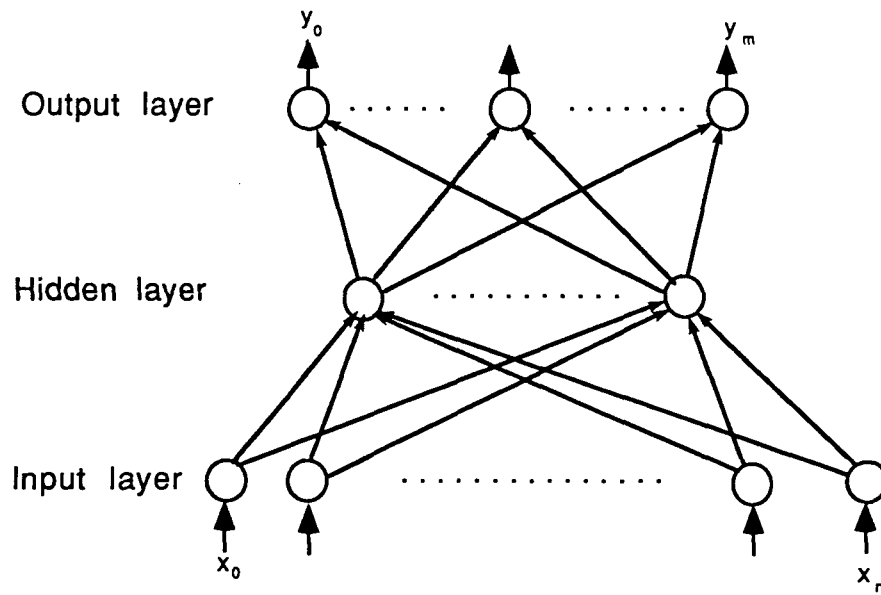


Figure 4.1: Multi-layer Perceptron

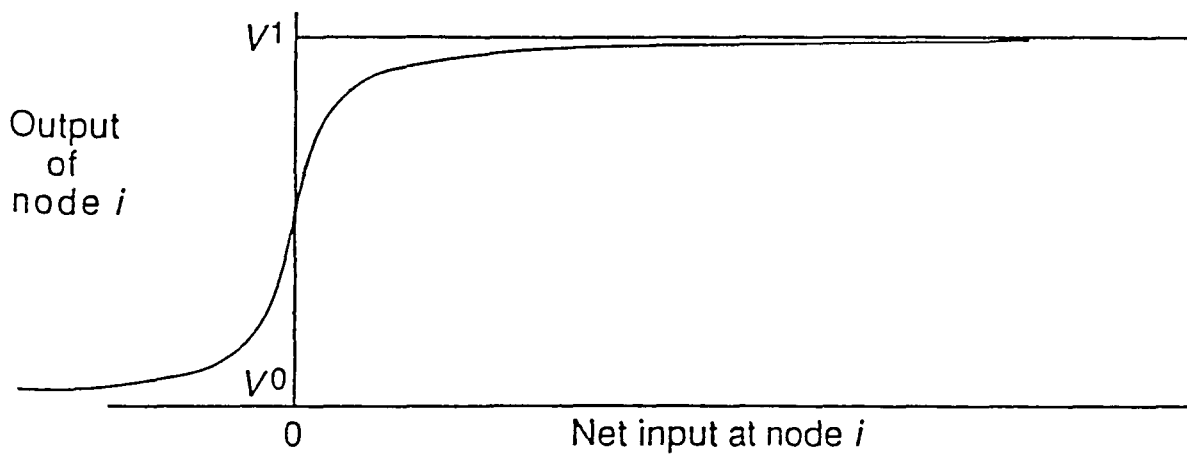


Figure 4.2: Sigmoidal function

classes represent different defect types, and the patterns represent parameterization of signals obtained using the eddy current technique.

The algorithm commonly used in training the perceptrons is the well-known *Back-Propagation Algorithm* which is described briefly next.

Back-Propagation Algorithm

The objective of the algorithm [27] and [28] is to minimize the error E between the output y computed by the network, and the desired output d , expressed by

$$E = \frac{1}{2} \sum_{l=1}^M \sum_{j=1}^N (y_{jl} - d_{jl})^2 \quad (4.1)$$

where j spans the output nodes and l spans the samples in the training set.

Differentiating (4.1) with respect to the nodal inputs and outputs

$$\frac{\partial E}{\partial y_j} = y_j - d_j \quad (4.2)$$

$$\frac{\partial E}{\partial x_j} = \frac{\partial E}{\partial y_j} \frac{\partial y_j}{\partial x_j} \quad (4.3)$$

where x_j is the input to node j . The transfer function of a node is taken to be a sigmoidal function, i.e for node j , the output y_j is related to the input x_j as:

$$y_j = \frac{1}{1 + \exp(-x_j)} \quad (4.4)$$

From (4.3), (4.4) we get:

$$\frac{\partial E}{\partial x_j} = \frac{\partial E}{\partial y_j} y_j (1 - y_j) \quad (4.5)$$

The derivative of E with respect to the weight w_{ij} from a node i to node j is given as:

$$\frac{\partial E}{\partial w_{ij}} = \frac{\partial E}{\partial x_j} \frac{\partial x_j}{\partial w_{ij}} \quad (4.6)$$

The input x_j to node j is the sum of weighted outputs of the lower layer of nodes,

$$x_j = \sum_i y_i w_{ij} \quad (4.7)$$

Therefore:

$$\frac{\partial x_j}{\partial w_{ij}} = y_i \quad (4.8)$$

From (4.6), we get:

$$\begin{aligned} \frac{\partial E}{\partial w_{ij}} &= \frac{\partial E}{\partial x_j} y_i \\ &= y_i (y_j(1 - y_j)(y_j - d_j) - \delta_j) \\ &= -y_i \delta_j \end{aligned} \quad (4.9)$$

The weight w_{ij} can be changed iteratively to minimize the error E according to the rule:

$$w_{ij}(k + 1) = w_{ij}(k) - \eta \frac{\partial E}{\partial w_{ij}} \quad (4.10)$$

η is a gain term. The iteration terminates when $\frac{\partial E}{\partial w_{ij}} = 0$, and the error is minimized.

The algorithm can be summarized by the following steps:

Step1: assume small random values for the weights.

Step2: apply first vector \underline{X}_1 for which desired output \underline{d} is known.

Step3: Calculate output vector \underline{Y} corresponding to this input.

Step4: Adjust weights as follows:

$$w_{ij}(k + 1) = w_{ij}(k) + \eta \delta_j x_i \quad (4.11)$$

x_i is either an output of node i , or is an input to the network.

If node j is an output node then:

$$\delta_j = y_j(1 - y_j)(d_j - y_j)$$

If node j is an internal or hidden node then:

$$\delta_j = x_j(1 - x_j) \sum_l \delta_l w_{jl}$$

where l goes over all nodes in the layers above node j .

Convergence is sometimes faster if a momentum term σ is added and weight changes are smoothed as follows:

$$w_{ij}(k+1) = w_{ij}(k) + \eta \delta_j x_j + \alpha(w_{ij}(k) - w_{ij}(k-1)) \quad (4.12)$$

where, $0 \leq \alpha \leq 1$, and k is the iteration number

Step 5: Repeat by going to step 2.

Hopfield Networks

In 1982, Hopfield presented the first kind of networks with the objective of introducing networks which exhibit collective computational abilities based on neurobiology. Hopfield later developed his first model of such neural networks which was digital and stochastic. He then extended the work to include continuous and deterministic networks. Hopfield networks are constructed from a large number of simple components which can be easily adapted for implementation using integrated circuit techniques. These networks are used in many applications, such as image restoration [29, 30]. The following sections discuss the Hopfield's stochastic, deterministic, and linear programming networks.

Stochastic Network

The first kind of Hopfield neural networks is a digital stochastic network [31] shown in Figure 4.3. The network consists of two state neurons where neuron “i” is fired if its input is larger than a threshold U_i . The output of each neuron is connected to the input of all other neurons, but not to its own input. The network is used to store information of n sets of states, and thus can be considered as an associative memory. The weight between neuron “i” and neuron “j” is determined according to:

$$T_{ij} = \sum_{s=1}^n (2v_i^s - 1)(2v_j^s - 1) \quad (4.13)$$

where s is the state, v_i is output of the i'th neuron.

This network is stochastic; each neuron samples its input at random times. It changes its output as follows:

$$\begin{aligned} v_i &\rightarrow v_i^0 \text{ if } \sum_{j \neq i} T_{ij} v_j + I_i < U_i \\ &\rightarrow v_i^1 \text{ if } \sum_{j \neq i} T_{ij} v_j + I_i > U_i \end{aligned} \quad (4.14)$$

Hopfield showed that the performance of the networks can be understood by considering one global function for the network known as energy function. Although the energy is a global quantity, each neuron is oblivious of the fact that its output follows a trajectory which causes minimization of the energy function. This is similar to the movement of gas particles from high to low density to increase the entropy of the system, while each particle is just governed by Newton's laws. The energy function “E” of the network is given as follows:

$$E = -\frac{1}{2} \sum_{j \neq i} \sum_i T_{ij} v_i v_j - \sum_i I_i v_i + \sum_i U_i v_i \quad (4.15)$$

The change ΔE in E due to a change Δv_i in a node i

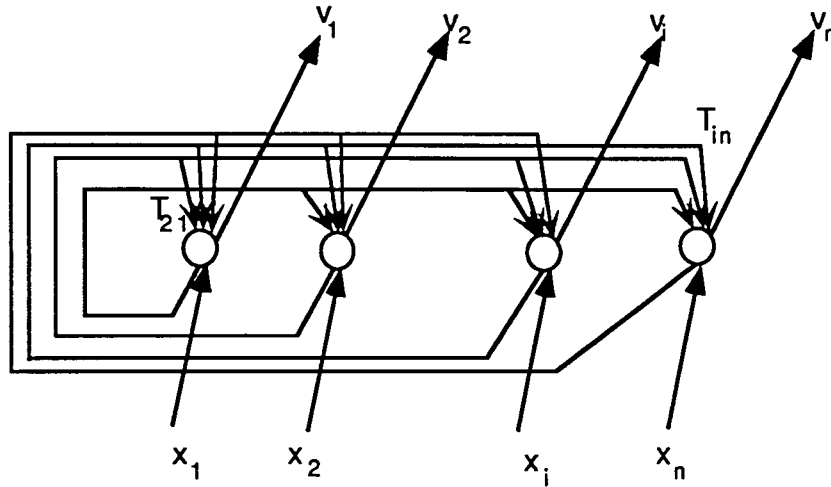


Figure 4.3: Hopfield stochastic network

$$\Delta E = -\left(\sum_{j \neq i} T_{ij} v_j + \sum_i I_i - \sum_i U_i\right) \Delta v_i \quad (4.16)$$

From (4.14) we see that ΔE is always negative.

$$\Delta E < 0$$

The input \underline{X} of the network (Figure 4.3) implies that we set the neuron outputs to values equal to \underline{X} at time ($t=0$). After convergence, the output \underline{v} of the neurons represents the nearest class, from the patterns used in training the network, to the pattern \underline{X} . Hopfield showed that for a network with n neurons, $0.15 n$ states can be remembered before error in recall is severe.

Deterministic Network

Hopfield also developed a deterministic network with continuous valued input and output [32]. The network is shown in Figure 4.4. The input of each amplifier is grounded through a resistor ρ_i and a capacitor C_i . The delay introduced by the RC circuit simulates the delay of the response of a biological neuron to a firing synapse. The output of neuron “i” is connected to the input of neuron “j” through a resistor R_{ij} . Since resistors cannot take negative values, a negated form of the output of each node is introduced at each amplifier. Should neuron “i” be excitatory to neuron “j”, the resistor R_{ij} is connected to the normal –positive– form of output of amplifier “i”. Otherwise, when the synapse is inhibitory, the resistor is connected to the negative form of the amplifier’s output.

Hopfield et al. showed [33] that a major goal of research in neuroscience is to provide systems that achieve “combination of power and speed,” that cannot be achieved by digital computers, but can be achieved easily in biological neural architectures. The computational power of biological networks comes from parallelism as in the mammalian visual systems. The power also comes from the large degree of feedback. The network was applied to solve the well known optimization problem of the *Traveling Salesman*. The network gives good results, as compared with those of the digital network which gives results that are little better than a random guess of the solution.

Hopfield also presented [34] the anatomy of a simple model of a neural circuit (Figure 4.6) which can be approximated by an analog neural network, assuming that the input current from all synapses are simply additive, and synaptic events are fast enough. In Figure 4.6, P’s are principal neurons and they have axons leaving the

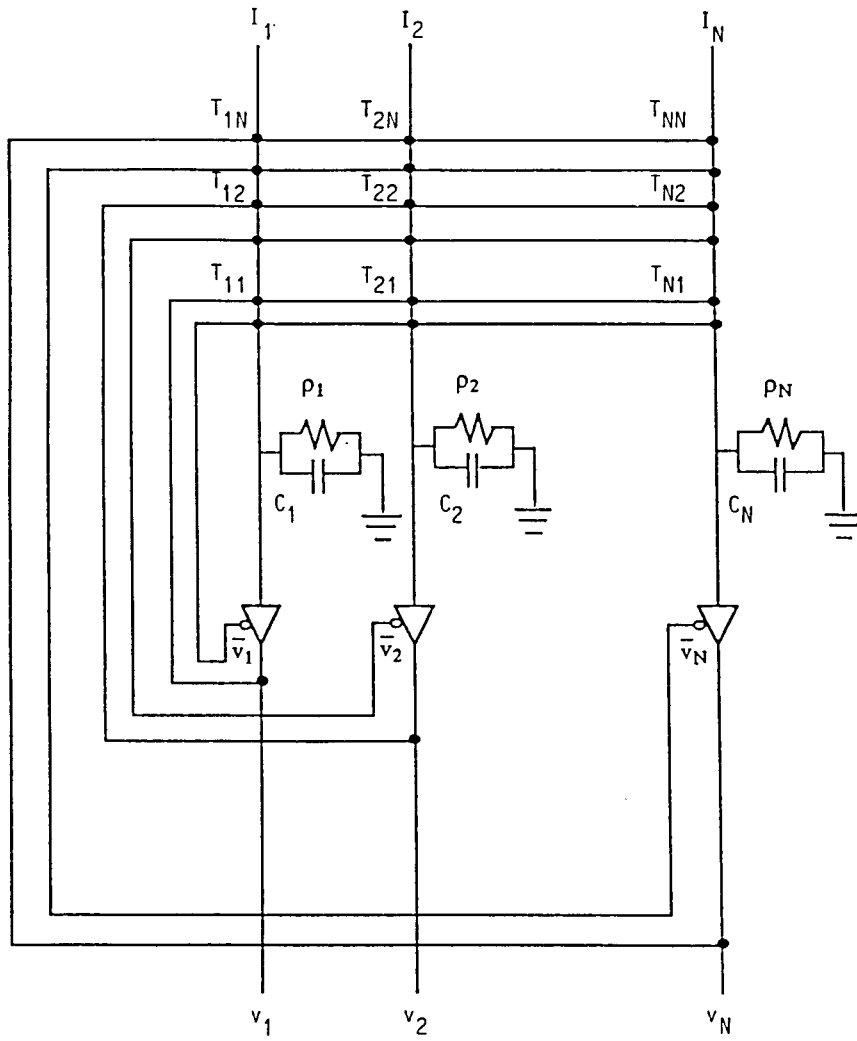


Figure 4.4: Hopfield continuous network

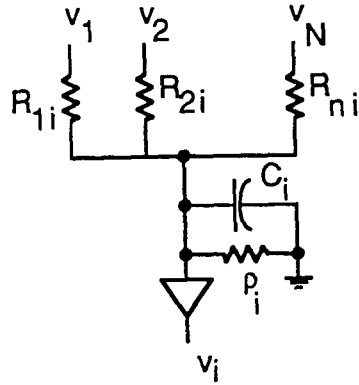
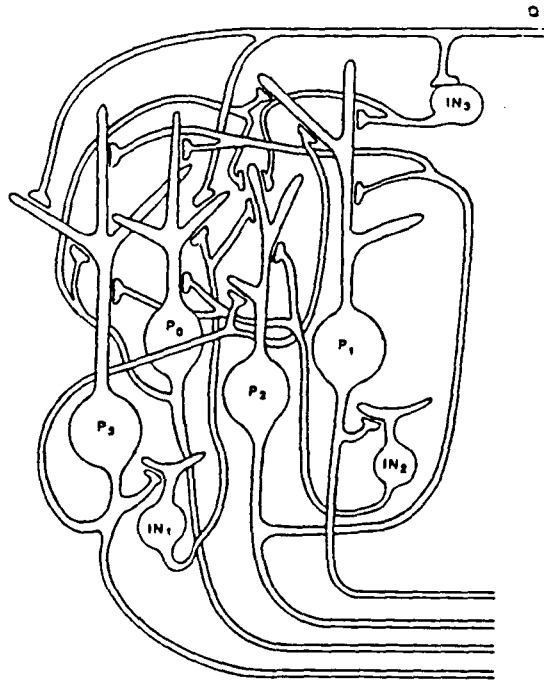
Figure 4.5: Neuron i 

Figure 4.6: Biological neural network

network as outputs. IN's are intrinsic neurons, and Q is an axon that brings external input to the neurons.

The network was used to accomplish different objectives by the proper choice of weights [35]. The energy function is formulated in such a way that the decrease in energy will move towards a stable state which satisfies the solution. The "T" matrix is then chosen to achieve this energy function. An analysis of the convergence property of the Hopfield network is presented below.

Analysis of the network Continuity of the current equation at input node of neuron "i" (Figure 4.5) can be written as follows:

$$C_i \frac{du_i}{dt} = \sum_j \frac{v_j - u_i}{R_{ij}} - \frac{u_i}{\rho_i} + I_i \quad (4.17)$$

where

- u_i is the input potential for amplifier i
- v_i is the output potential for amplifier i
- I_i is the external input current for amplifier i

Equation (4.17) can be written in the form

$$C_i (du_i/dt) = \sum_j T_{ij} v_j - u_i/R_i + I_i \quad (4.18)$$

where: $1/R_i = 1/\rho_i + 1/\sum_j R_{ij}$

The weight T_{ij} represents a conductance connecting neurons i and j.

The output voltage v_i of neuron i is related to its input u_i by the relationship,

$$v_i = s(u_i)$$

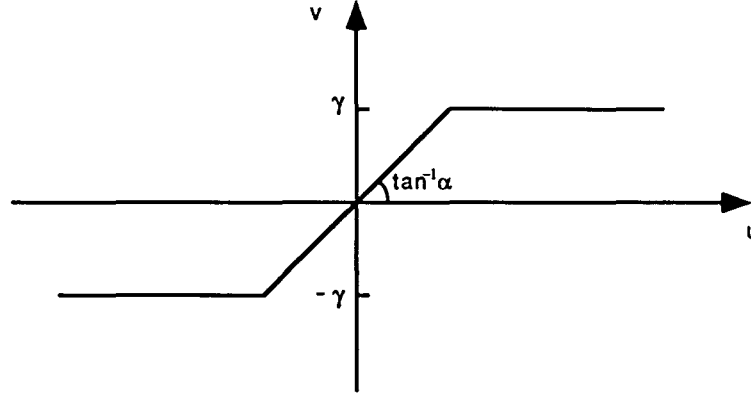


Figure 4.7: Transfer function of amplifier

Hopfield chose the function s to be a sigmoidal function. A simplified form of the transfer function shown in Figure 4.7 was suggested [30] as follows:

$$s_i = \begin{cases} \alpha u_i & |u_i| \leq \gamma/\alpha \\ \gamma & u_i > \gamma/\alpha \\ -\gamma & u_i < -\gamma/\alpha \end{cases} \quad (4.19)$$

where γ is chosen large enough to avoid saturation.

The energy function of the network is given as:

$$E = -\frac{1}{2} \sum_i \sum_j T_{ij} v_i v_j + \sum_i \frac{1}{R_i} \int_0^{v_i} s_i^{-1}(\xi) d\xi - \sum_i I_i v_i \quad (4.20)$$

Hopfield [32] showed that as the amplifier gain goes to infinity, this continuous network with symmetric T will have stable states that correspond to corners of a hypercube, i.e. the stable states of a digital-stochastic network. For finite gain, the second term in the right hand side of equation (4.20) becomes significant, and the minima are displaced from the corners towards the interior of the cube.

Equations (4.18), and (4.20) can be written in vector form as follows:

$$C \frac{d\mathbf{u}}{dt} = T\mathbf{v} - R^{-1}\mathbf{u} + \mathbf{I} \quad (4.21)$$

$$E = -\frac{1}{2}\mathbf{v}^T T\mathbf{v} + \mathbf{r}^T \hat{\mathbf{S}} - \mathbf{v}^T \mathbf{I} \quad (4.22)$$

where:

$$C := \text{diag}[C_1, C_2, \dots, C_n], R := \text{diag}[R_1, R_2, \dots, R_n]$$

$$\hat{\mathbf{S}}_i := \int_0^{v_i} s_i^{-1}(\xi) d\xi$$

$$r_i := 1/R_i$$

For symmetric T we get:

$$\begin{aligned} \nabla E &= -T\mathbf{v} + R^{-1}\mathbf{u} - \mathbf{I} \\ &= -C \frac{d\mathbf{u}}{dt} \end{aligned} \quad (4.23)$$

The time derivative of E will be given as:

$$\begin{aligned} \frac{dE}{dt} &= \dot{\mathbf{v}}^T \nabla E(\mathbf{v}) \quad (\text{chain rule}) \\ &= -C \dot{\mathbf{v}}^T \dot{\mathbf{u}} \\ &= -C \check{\mathbf{S}}^T(\mathbf{v}) \dot{\mathbf{v}} \end{aligned} \quad (4.24)$$

where:

$$\begin{aligned} \check{\mathbf{S}} &= \left[\frac{d}{dv_1} s_1^{-1}(v_1), \frac{d}{dv_2} s_2^{-1}(v_2), \dots, \frac{d}{dv_n} s_n^{-1}(v_n) \right]^T \\ \dot{v}_i &= \dot{v}_i^2 \end{aligned} \quad (4.25)$$

Since we choose $s_i^{-1}(v_i)$ to be a monotonic increasing function, from equation (4.24) we can conclude that (dE/dt) will always be negative. Thus, the network will converge to a minimum of E and will not oscillate.

In [36] some theoretical results governing the dynamics of the network were presented. Two of these theorems are presented here, and are used in determining the parameters of the transfer function of the amplifiers (α, γ) in equation (4.19). The first theorem relates the norm of \underline{u} with γ , elements of \mathbf{T} matrix, and input vector \underline{I} . This result can be used to choose the value of γ .

Theorem: All trajectories of output vector \underline{v} converge to a bounded region in the state space.

Proof: Consider the function $W(\underline{u}) = \frac{1}{2} \underline{u}^T R C \underline{u}$

$$\begin{aligned} \dot{W}(\underline{u}) &= \underline{u}^T R C \dot{\underline{u}} \\ &= \underline{u}^T R (-R^{-1} \underline{u} + T \underline{v} + \underline{I}) \\ &\leq -\|\underline{u}\|^2 + \|\underline{u}\| \|\underline{RL}\| \\ &= -\|\underline{u}\| [\|\underline{u}\| - \|\underline{RL}\|] \end{aligned}$$

where: $L_i := \gamma \sum_j |T_{ij}| + |I_i|$

Hence $\dot{W}(u) < 0$ for \underline{u} outside the sphere defined by:

$$\rho_u = \{\underline{u} \in U^n, \|\underline{u}\| < \|\underline{RL}\|\}$$

The value of γ is chosen such that the required the final values of \underline{u} belong to the space U^n .

The second theorem relates to the stability of point ($\underline{v} = 0$). We need the point ($\underline{v} = 0$) to be unstable so that the output will converge to a solution. The relation between amplifier inputs and outputs can be expressed in matrix form as:

$$\underline{u} = \hat{S}(\underline{v}) \quad (4.26)$$

From (4.21), and (4.26), we get:

$$C \frac{d}{d\underline{v}} \hat{\underline{S}}(\underline{v}) \dot{\underline{v}} = T\underline{v} - R^{-1} \hat{\underline{S}}(\underline{v}) + \underline{I}$$

Using the notation:

$$\underline{C}(\underline{v}) := C \frac{d}{d\underline{v}} \hat{\underline{S}}(\underline{v})$$

$$\underline{F}(\underline{v}) := R^{-1} \hat{\underline{S}}(\underline{v})$$

we get:

$$\dot{\underline{v}} = \underline{C}^{-1}(\underline{v}) [T\underline{v} - \underline{F}(\underline{v}) + \underline{I}] \quad (4.27)$$

Expanding the function \underline{v} around an equilibrium point v^i we get:

$$\dot{\underline{v}} = \underline{C}^{-1}(v^i) [T - D_1 \underline{F}(v)] \tilde{\underline{v}} \quad (4.28)$$

where D_1 is first order differential operator

Considering the case where we have identical amplifiers with transfer function given in (4.19). With identical values of C and ρ , we get:

$$\begin{aligned} \underline{C}(\underline{v}) &= C \mathcal{I} \frac{d}{d\underline{v}} \hat{\underline{S}}(\underline{v}) \\ &= C \frac{1}{\alpha} \mathcal{I} \\ D_1 \underline{F}(\underline{v}) &= R^{-1} \mathcal{I} \frac{d}{d\underline{v}} \hat{\underline{S}}^T(\underline{v}) \\ &= \frac{1}{\alpha} R^{-1} \end{aligned}$$

where \mathcal{I} is the identity matrix.

From (4.28), we get:

$$\begin{aligned} \dot{\underline{v}} &= \underline{C}^{-1}(v^i) [T - D_1 \underline{F}(v)] \tilde{\underline{v}} \\ &= \frac{\alpha}{C} [T - \frac{1}{\alpha} R^{-1} v^T \mathcal{I}] \tilde{\underline{v}} \end{aligned}$$

For symmetric T , we have

$$\begin{aligned}\dot{\underline{v}} &= \frac{\alpha}{C} [P\Lambda P^T - \frac{1}{\alpha} R^{-1} \underline{v}^T P P^T] \underline{v} \\ &= \frac{\alpha}{C} P[\Lambda - \frac{1}{\alpha} R^{-1}] P^T \underline{v}\end{aligned}\quad (4.29)$$

where, $P := [e_1, e_2, \dots, e_n]$ and e_i is an orthonormal eigenvector of matrix T .

$\Lambda := \text{diag} [\lambda_1, \lambda_2, \dots, \lambda_n]$, λ_i is an eigenvalue of T .

From (4.29), point ($\underline{v} = 0$) will be unstable if for any i , $1 \leq i \leq n$:

$$\lambda_i > \frac{1}{\alpha R_i} \quad (4.30)$$

Equation (4.30) can be used in determining an appropriate value for α .

Linear Programming Network

Linear programming networks are described in [35], where the minimization of cost function is performed subject to linear constraints:

$$D\underline{v} \geq \underline{B}$$

In the network shown in Figure 4.8, the response time of “f” amplifiers is negligible compared to “s” amplifiers.

The differential equation describing the dynamics of the networks can be written in the form [35]:

$$\begin{aligned}C \frac{d\underline{u}}{dt} &= D^T f(\underline{v}) - R^{-1} \underline{u} + \underline{I} \\ &= D^T f(D\underline{v} - \underline{B}) - R^{-1} \underline{u} + \underline{I}\end{aligned}\quad (4.31)$$

The energy function of the network is given as:

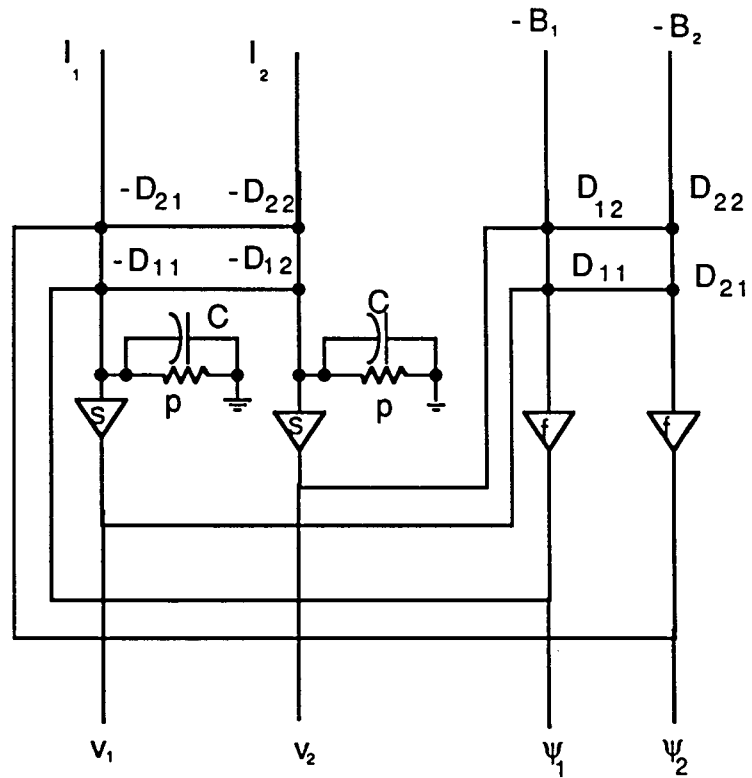


Figure 4.8: Linear programming network

$$E = \underline{a}^T \underline{\mathcal{F}}(D\underline{v} - \underline{B}) + \underline{r}^T \underline{\hat{S}} - \underline{v}^T \underline{I} \quad (4.32)$$

where:

$$\underline{a}^T = [1 \ 1 \ \dots \ 1]$$

$$\underline{\mathcal{F}}_i := \int_0^{v_i} f_i(\xi) d\xi$$

$$\underline{\hat{S}}_i := \int_0^{v_i} s_i^{-1}(\xi) d\xi$$

Therefore :

$$\nabla E = -C \frac{d\underline{u}}{dt}$$

$$\begin{aligned} \frac{dE}{dt} &= \underline{\dot{v}}^T \nabla E(\underline{v}) \\ &= -C \underline{\dot{v}}^T \underline{\dot{v}} \\ &= -C \underline{\check{S}}^T(\underline{v}) \underline{\dot{v}} \end{aligned} \quad (4.33)$$

Where: $\underline{\check{S}}$, and $\underline{\dot{v}}$ are given in (4.25).

Equation (4.33) is similar to (4.24), indicating that the derivative of the energy function of a linear programming network is also negative. Thus, the network will converge towards a minimum of the energy function and will not oscillate.

An algorithm for solving inverse problems using neural networks is presented in the following chapter.

CHAPTER 5. APPLICATION OF NEURAL NETWORKS FOR SOLVING INVERSE PROBLEMS

This chapter discusses solution of inverse problems expressed in the form of Fredholm integral equation using the neural networks described in Chapter 4. Section 1 describes the use of the perceptron network with two illustrative examples. Section 2 describes a method for solving the inverse problem by casting the problem as an exercise in energy function minimization and using the Hopfield network as an energy minimization tool.

Solution of Inverse Problems Using the Perceptron

An inverse problem described by Fredholm Integral equations [37] was first chosen. The multilayer perceptron network is trained with a priori known solution, for a clean version of input, using the back-propagation algorithm. In the testing phase, a noisy input function was applied and the network was used to compute the solution of the inverse problem.

The back propagation algorithm described in Chapter 4 which is used for training perceptrons has two major problems:

1. The algorithm is sometimes trapped in the local minima of the squared error function.

2. The weight coefficients after training are different, depending on the network configuration, and the initial values of weights.

A simple solution to these problems is to use a number of networks each operating with different initial weights and then compute the average of their outputs [37].

Results

The algorithm was applied to two examples of Fredholm integral equations used by Phillips [5]. The inverse problem solution is very sensitive to the noise in the input. In the numerical solution, the truncation error is treated as a source of noise. The solution obtained by Phillips is seen to be very sensitive to the value of the regularization factor, and the truncation error.

Example 1 The integral equation is of the form

$$\int_{-3}^3 k(x-y)z(x)dx = u(y)$$

where:

$$\begin{aligned} k(\xi) &= 1 + \cos \frac{\pi\xi}{3} & |\xi| \leq 3 \\ &= 0 & |\xi| > 3 \\ u(\lambda) &= (6 - |\lambda|)(1 - \frac{1}{2} \cos \frac{\pi\lambda}{3}) + \frac{9}{2\pi} \sin \frac{\pi|\lambda|}{3} & |\lambda| \leq 6 \\ &= 0 & |\lambda| > 6 \end{aligned}$$

In order to train the neural network, $u(y)$ was sampled at 4 points to obtain the input vector with 25 samples of solution $z(x)$ representing the output vector.

Networks of the following configuration were used:

4 nodes for the input layer.

10 nodes for the hidden layer.

25 nodes for the output layer.

The networks were trained starting from four different initial weights. The performance of the networks was then tested using 200 vectors of $u(y)$ corrupted by noise with the signal to noise ratio set at 20 dB. The final output was taken to be the average of the four network outputs. The average and the standard deviation of the 200 output vectors were estimated. In Figure 5.1 the solid curve shows the true values of $z(x)$, and the '+' signs show the range of the standard deviation of the neural network solutions about the average values.

Example 2 The integral equation is given as

$$\int_{-30}^{30} k(x-y)z(x)dx = u(y)$$

where the numerical values of $k(\xi)$ and $u(\lambda)$ are depicted in Figure 5.2.

A neural network with 16 input nodes, 10 hidden nodes, and 31 output nodes was trained with four different initial weights.

The network was then tested with 200 vectors of noisy $u(y)$ with the SNR at 20 dB. As in example 1, the solution was considered to be the average of 4 different network outputs corresponding to the different initial values for weights. Average and standard deviation of the output vectors were estimated. A plot of the true value of $z(x)$ and neural network range of solution are shown in Figure 5.3.

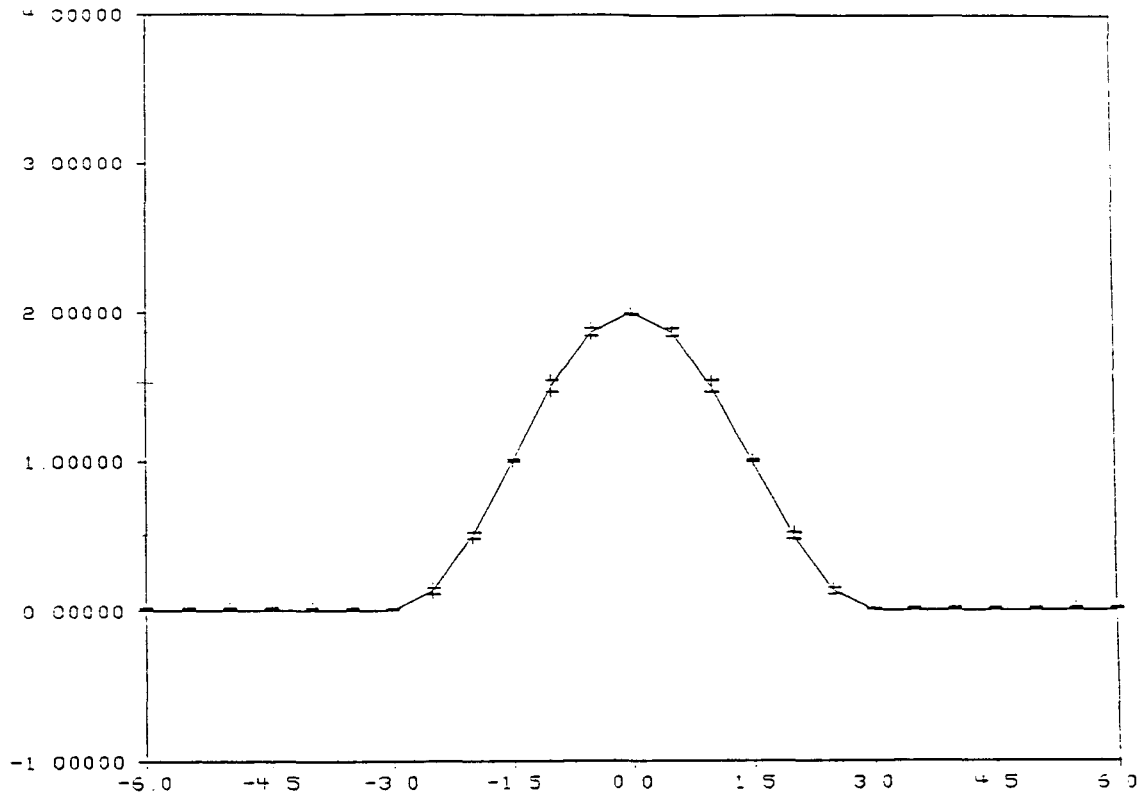


Figure 5.1: True value for $z(x)$ and range of neural network solution for example 1

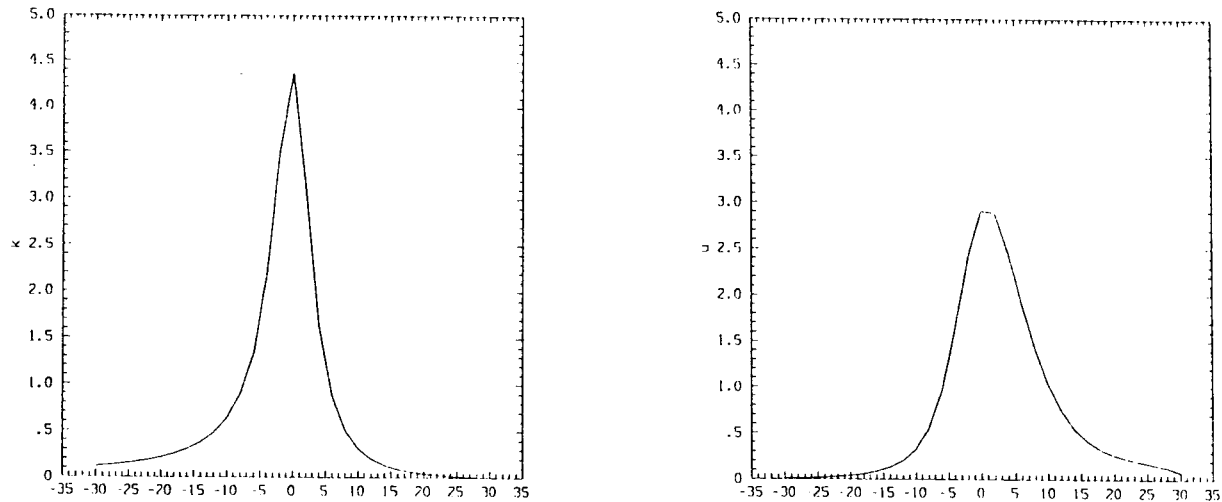


Figure 5.2: Kernel $k(\xi)$ and input $u(\lambda)$ for example 2

Application: Flow Measurements

One of the applications of this algorithm is in the measurement of fluid flow in open and closed conduits. Although measurements of fluid flow can be obtained easily by using simple meters, they are often inaccurate. Accurate measurements require the use of more sophisticated instrumentation. As an example, the flux can be measured in closed conduits using differential pressure meters such as the orifice, or flow velocity meters such as the Pitot tube. In the case of open channels, the flow can be measured using weirs or current meters.

A simpler method for measuring the flow is to employ non-intrusive methods which involve the use of electromagnetic, or ultrasonic flowmeters [38]. Models of ultrasonic meters that are used for flow measurements in pipelines and open channels are described in [39].

One way of measuring the flow using ultrasonic methods is to measure the travel

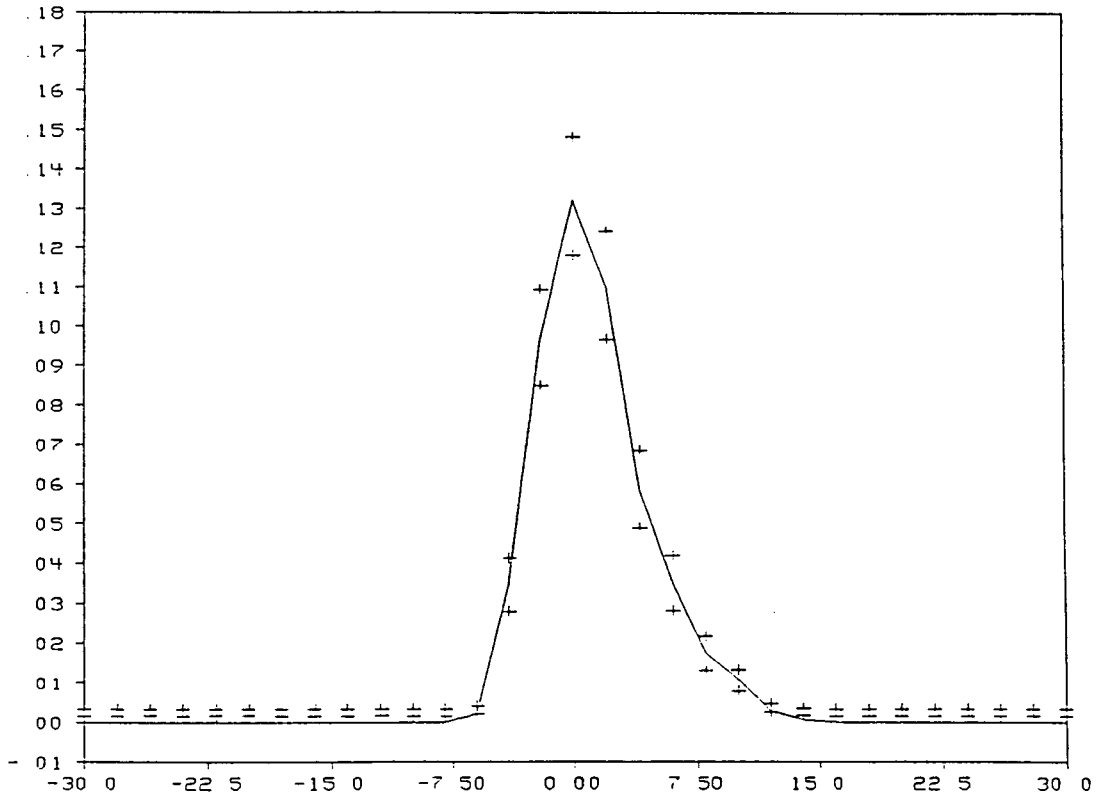


Figure 5.3: True value of $z(x)$ and range of neural network solution for example 2

time (t_u) of a pulse traveling upstream, and the travel time(t_d) of a pulse traveling downstream (Figure 5.4). The flow velocity is then given by [39]:

$$u_f = \frac{L^2 + D^2}{2L} \left[\frac{1}{t_u} - \frac{1}{t_d} \right]$$

where L is the axial distance between the two transducers, and D is the diameter of the pipe.

The flow Q is expressed as:

$$Q = u_m A \quad (5.1)$$

where, u_m is the mean velocity, and A is the cross sectional area.

u_m is related to u_f by the following relation [39]:

$$u_m = u_f \frac{\int_0^1 u(r) d(2r/D)^2}{\int_0^1 u(r) d(2r/D)} \quad (5.2)$$

where $u(r)$ is the velocity value at radius r .

From (5.2), we can write u_m as

$$u_m = u_f C \quad (5.3)$$

where the calibration factor C has to be determined. This factor depends on the velocity profile which, in turn, depends on the configuration of the flow conduit. The calibration factor C is very sensitive to changes in the velocity profile, and can be affected even by a change in the roughness of the wall.

A neural network approach can be used for solving this problem. The network can be trained as shown in the last two examples using input data of travel time corresponding to different cords or diagonals, and output corresponding to the discharge value obtained by a conventional method. The advantage of using the neural network

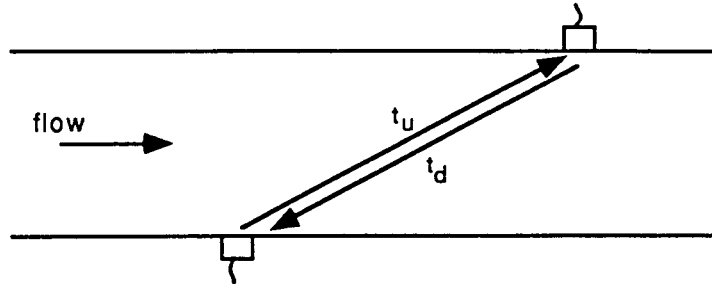


Figure 5.4: Ultrasonic measurement of flow

is that the ultrasonic flow meter can be calibrated using accurate instrumentation in field, and then used to obtain reliable measurements without the need for using such instrumentation in daily usage.

Solution of Inverse Problems Using Hopfield Network

An alternate approach for solving Fredholm integral equations is offered by Hopfield networks. In order to formulate the integral equation in a suitable framework, the system parameters function $z(s)$ in equation (2.9) is first represented [40] as

$$z(x) = \sum_{i=1}^N V_i R_i(x) \quad (5.4)$$

where R_i is a basis function, and we can take it to be sine, and cosine functions.

The Fredholm integral equation can therefore be represented in discrete form by

the matrix equation

$$F\underline{V} = \underline{g} + \underline{n} \quad (5.5)$$

where,

$$F_{ij} = \int_a^b k(x, y_j) R_i(x) dx$$

$$g_i = u(x_i)$$

and \underline{n} represents the noise.

The solution of (5.5) can be obtained by minimizing an error function of the form:

$$E = \frac{1}{2} (F\underline{V} - \underline{g})^T (F\underline{V} - \underline{g}) + \lambda \underline{V}^T D \underline{V} \quad (5.6)$$

The second term in (5.6) is a regularization term and is chosen to be a smoothness constraint on the solution. The parameter λ is the Lagrange multiplier. The value of this parameter can be obtained if the norm of the noise \underline{n} is known. An iterative algorithm for determining the value of λ is given in [41, 42].

To impose the smoothness constraint on the solution, the matrix D is chosen as:

$$D = \text{diag}[d_1, d_2, \dots, d_N]$$

where $d_i = \int_a^b R_i''(x) dx$. If we choose R_i to be a cosine function for even i , and a sine function for odd i , then:

$$d_i = \begin{cases} \left[\frac{\pi}{L} \frac{1}{2}(i-1) \right]^4 & i = 1, 3, \dots \\ \left[\frac{\pi}{L} \frac{1}{2}(i) \right]^4 & i = 2, 4, \dots \end{cases}$$

where L is the interval of integration.

Another constraint can be added to the error function using the boundary condition. If the value of $z(x)$ is known at a certain point p , we have

$$\Psi \underline{V} = z_p \quad (5.7)$$

where elements of matrix Ψ are basis functions R . In general, z_p can be a complex quantity. For example, in electromagnetic inverse problem z represents the complex permittivity ϵ_c . For this problem, we have

$$z_p = [\epsilon_p \quad \sigma_p/\omega\epsilon_0]^T$$

$$\Psi_{1i} = \begin{cases} R_i(x_p), & 1 \leq i \leq N \\ 0 & N < i \leq 2N \end{cases}$$

$$\Psi_{2i} = \begin{cases} 0 & 1 \leq i \leq N \\ R_{(i-N)}(x_p), & N < i \leq 2N \end{cases}$$

R_i is a basis function.

The error function indicating this constraint can be written as:

$$E = \frac{1}{2}(F\underline{V} - \underline{g})^T(F\underline{V} - \underline{g}) + \lambda\underline{V}^T D\underline{V} + \lambda_1(\Psi\underline{V} - \underline{\psi}_p)^T(\Psi\underline{V} - \underline{\psi}_p) \quad (5.8)$$

The dynamic terms that depends on \underline{V} in (5.8) can be written in the form:

$$E = -\frac{1}{2}\underline{V}^T T^\dagger \underline{V} - \underline{V}^T \underline{I}^\dagger \quad (5.9)$$

where:

$$T^\dagger = -F^T F - \lambda D - \lambda_1 \Psi^T \Psi$$

$$\underline{I}^\dagger = F^T \underline{g} + 2\lambda_1 \Psi^T \underline{\psi}_p$$

Equation (5.9) can be compared with the energy function of neural network given in (4.22) to obtain the values for the resistor weights, and the external input current

to the neural network. For the case of a neural network with amplifiers that have the transfer function given in (4.19), the network energy function can be written as:

$$E = -\frac{1}{2}\underline{V}^T T \underline{V} + \frac{1}{2}\underline{V}^T T_r \underline{V} - \underline{V}^T \underline{I} \quad (5.10)$$

where:

$$T_r := \text{diag}[1/(\alpha_1 R_1) \ 1/(\alpha_2 R_2) \ \dots \ 1/(\alpha_n R_n)]$$

α_i is gain of amplifier i , and R_i is input resistance to amplifier i .

From (5.9) and (5.10), we get:

$$\begin{aligned} T &= T^\dagger + T_r \\ \underline{I} &= \underline{I}^\dagger \end{aligned}$$

We use the circuit as shown in Figure 5.5. The energy minimization network is given in Figure 4.4, and the linear programming network is shown in Figure 4.8. The input \underline{u} of amplifiers of the minimization network is connected to external input \underline{I} for the linear programming network through a switch. The output $\underline{\psi}$ of linear programming network is connected to input \underline{I} of minimization network. The inputs \underline{B} in Figure 4.8 are chosen to be equal to \underline{g} of equation (5.5), and the weights D of the network are obtained from F in equation (5.5). The transfer function of s amplifiers of the linear programming network is similar to the transfer function of energy minimization network. The transfer function of f amplifiers of the linear programming network is chosen as:

$$\psi_j = f(z_j)$$

where:

$$f(z) = \begin{cases} 0 & -\epsilon \leq z \leq \epsilon \\ -z & z \leq -\epsilon, \ z \geq \epsilon \end{cases}$$

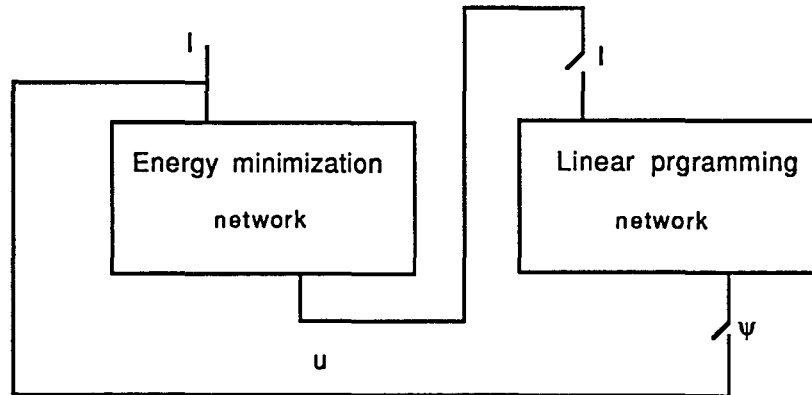


Figure 5.5: Neural network with feedback circuit

The linear programming circuit will give 0 output when

$$-\epsilon \leq (F\underline{V} - \underline{g}) \leq \epsilon \quad (5.11)$$

The switches between the two networks are left off for a period of few time constants of the minimization network. The switches are then turned on. If the minimization network is trapped in a local minimum, the output ψ of the linear programming network will excite the minimization network again and move the energy function away from the local minimum. When condition (5.11) is satisfied, both networks will stop, and the output of the energy minimization network is the desired solution.

Simulation of Energy Minimization

A modified gradient descent algorithm is used to simulate the minimization of the energy function. Gradient descent algorithms depend on starting with an initial

value of V , and iteratively changing V , such that,

$$V = V + \mu \nabla E$$

μ is a small number that determines the step size, and ∇E can be obtained from (5.9)

$$\nabla E = -T^\dagger \underline{V} - \underline{I}^\dagger$$

The iterations will stop when the gradient of E becomes sufficiently small.

A modification for the steepest-descent algorithm is shown in [43]. We update \underline{V} such that, at iteration $(r+1)$, V_i is given in terms of V_i at iteration r as follows:

$$V_i^{r+1} = V_i^r + \mu^r \delta_i^r$$

where δ_i is given by [43]

$$\delta_i = \frac{[1 + (v_i^r)^2] (\frac{\partial E}{\partial v_i})^r}{\left[\sum_{j=1}^N \left([1 + (V_j^r)^2] (\frac{\partial E}{\partial v_j})^r \right)^2 \right]^{\frac{1}{2}}}$$

The modified gradient descent procedure is summarized by the following steps.

1. Choose a certain value for μ
2. Calculate E^r , and $\delta_1^r, \dots, \delta_n^r$
3. Calculate E_{temp} which is the energy corresponding to $(V_i^r + \mu^r \delta_i^r)$.

If $E_{temp} > E^{r-1}$ then:

$$\mu = \mu/4$$

go to step 2

4. Calculate the cosine of the angle θ between the vectors $\underline{\delta}^r$ and $\underline{\delta}^{r-1}$.

$$\cos \theta = \sum_{j=1}^N \delta_j^{r-1} \delta_j^r$$

5. If $\cos \theta < 0$, then:

$$\mu = \mu/4$$

go to step 2

6. Calculate μ^{r+1}

$$\mu^{r+1} = \mu^r (.5 + \cos^4 \theta)$$

7. If δ_i for all i is less than a small number δ :

then:

terminate;

else:

increment r , and go to step 2.

An application of this algorithm to inverse problems in geophysics is presented in the next chapter, where a Hopfield network is developed for inverting electromagnetic scattering data from layered media.

CHAPTER 6. INVERSE PROBLEM OF SCATTERING FROM LAYERED MEDIA

We consider here the problem of one-dimensional profile inversion. We first discuss the case of a horizontally stratified media, and then describe the problem of cylindrically stratified media. Both cases lead to a Fredholm integral equation of the first kind that can be solved using a neural network. Simulation results of neural network implementation are then presented.

Horizontally Stratified Media

In this case we assume that the media consist of n layers, where layer i has conductivity σ_i , as shown in Figure 6.1. The transmitter is a horizontal circular loop, situated on or above the surface of first layer. When the measurements are taken at the center of the loop, the process is known as *central induction sounding*; and when the measurements are taken outside the loop the method is called *induction depth sounding*. The problem of horizontally stratified media has been solved in [18] using the method of Backus and Gilbert.

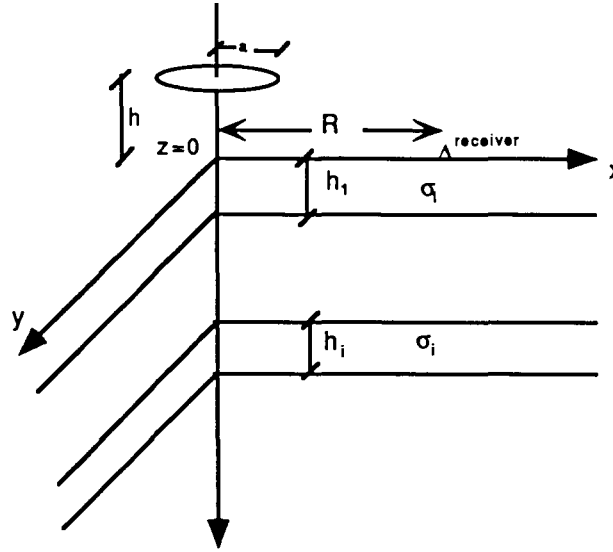


Figure 6.1: Horizontally stratified slab

Forward Problem

The circular symmetry of the problem allows us to use cylindrical coordinates. It can be shown [44] that the electric field components E_r , E_z , and the magnetic field component H_ϕ vanish for this geometry. We can write Maxwell's curl equations in the i 'th layer in the following forms [45]:

$$\frac{\partial E_\phi}{\partial z} = j\omega\mu_i H_r \quad (6.1a)$$

$$\frac{1}{r} \frac{\partial}{\partial r} (r E_\phi) = -j\omega\mu_i H_z \quad (6.1b)$$

$$\frac{\partial H_r}{\partial z} - \frac{\partial H_z}{\partial r} = (j\omega\mu\epsilon_i + \sigma_i) E_\phi + J_{s\phi} \quad (6.1c)$$

where $J_{s\phi}$ is the source current density given by:

$$\underline{J}_{s\phi} = \frac{I(\omega)a\delta(r-a)\delta(z+h)}{r} \hat{a}_\phi \quad (6.2)$$

We can get the inhomogeneous scalar wave equation of the primary (incident) field E_{ϕ_p} , or simply E_p , from equations (6.1a), (6.1b), and (6.1c)

$$\left(\frac{\partial^2}{\partial r^2} + \frac{1}{r} \frac{\partial}{\partial r} - \frac{1}{r^2} + \frac{\partial^2}{\partial z^2} + k^2\right) E_p(r, z, \omega) = \frac{j\omega\mu_0 I(\omega) \delta(r-a) \delta(z+h)}{r} \quad (6.3)$$

The solution of the wave equation is obtained [46] by taking the Hankel transform of (6.3). Hankel transform is defined as:

$$\begin{aligned} \mathcal{H}[F(r)] &= \int_0^\infty F(r) J_1(\lambda r) r dr = F(\lambda) \\ \mathcal{H}^{-1}[F(\lambda)] &= \int_0^\infty F(\lambda) J_1(\lambda r) \lambda d\lambda = F(r) \end{aligned}$$

The Hankel transform of E_p is given by:

$$E_p(\lambda, z, \omega) = -\frac{j\omega\mu_0 a I(\omega)}{2} J_1(\lambda a) \frac{e^{-u_0(z+h)}}{u_0} \quad (6.4)$$

where: $u_i = (\lambda^2 - k_i^2)^{\frac{1}{2}}$

From Boundary conditions at $z=0$ for electric and magnetic fields, the total electric field (incident and reflected) is shown to be:

$$E(r, z=0, \omega) = -j\omega\mu_0 a I(\omega) \int_0^\infty \frac{e^{-u_0 h}}{u_0} \frac{Z^1}{Z_0 + Z^1} J_1(\lambda a) J_1(\lambda r) \lambda d\lambda \quad (6.5)$$

where:

Z_i is input impedance of layer i, and is given by:

$$\begin{aligned} Z_i &= \left. \frac{E(\lambda, \omega)}{H_r(\lambda, \omega)} \right|_{\text{at surface of layer i}} \\ &= -\frac{j\omega\mu_i}{u_i} \end{aligned} \quad (6.6)$$

and Z^i is given by:

$$Z^i = Z_i \frac{Z^{i+1} + Z_i \tanh u_i h_i}{Z_i + Z^{i+1} \tanh u_i h_i} \quad (6.7)$$

Ryu et al. [45] showed that the integral in (6.5) is improper because of the Bessel function, especially for large λ since:

$$\lim_{\lambda \rightarrow \infty} \frac{e^{-u_0 z}}{u} \frac{Z^1}{Z_0 + Z^1} J_1(\lambda a) J_1(\lambda r) \lambda \rightarrow \frac{e^{-\lambda z}}{2} J_1(\lambda a) J_1(\lambda r)$$

Expressing E as

$$E(r, z, \omega) = -j\omega\mu_0 aI(\omega) \left\{ \int_0^\infty \left(\frac{e^{-u_0 z}}{u_0} \frac{Z^1}{Z_0 + Z^1} \lambda - \frac{e^{-\lambda z}}{2} \right) J_1(\lambda a) J_1(\lambda r) d\lambda + \int_0^\infty \frac{e^{-\lambda z}}{2} J_1(\lambda a) J_1(\lambda r) d\lambda \right\} \quad (6.8)$$

$$= -j\omega\mu_0 aI(\omega) \left\{ \int_0^\infty \left(\frac{e^{-u_0 z}}{u_0} \frac{Z^1}{Z_0 + Z^1} \lambda - \frac{e^{-\lambda z}}{2} \right) J_1(\lambda a) J_1(\lambda r) d\lambda + \frac{ar}{2\pi} \int_{-1}^1 \text{Real} \left[\frac{(1-x^2)^{1/2}}{z^2 + 2jazz - z^2x^2 + r^2} \right] dx \right\} \quad (6.9)$$

H_r and H_z can be deduced from E_ϕ using (6.1a) and (6.1b)

Inverse Problem:

Recall from Chapter 3 the integral equation :

$$f_s(\underline{r}) = \int_{vol} G(\underline{r} - \underline{r}') O(\underline{r}') f(\underline{r}') d\underline{r}' \quad (6.10)$$

For the low frequency range that is used in this configuration, permittivity ϵ has a small effect on the field, as compared to that of σ . We can assume that the change in field is only due to change in σ . If we consider that the field corresponding to $\sigma(z)$ is E , and field corresponding to $(\sigma(z) + \delta\sigma(z))$ is E^\dagger then from (6.10) we have

$$\delta E(\rho, z = 0) = \int_0^\infty dz' k_0^2 \frac{-j\delta\sigma(z')}{\omega\epsilon_0} \int_0^\infty d\rho' G(\rho - \rho', z') E^\dagger(\rho', z' + h) \quad (6.11)$$

Transforming to Hankel- λ space, we get:

$$\delta E(\lambda, h, \omega) = -j\omega\mu \int_0^{\infty} dz' \delta\sigma(z') G(\lambda, z') E^\dagger(\lambda, z' + h) \quad (6.12)$$

The Green's function can be obtained in terms of $E(\lambda, z')$, as will be shown later. Also, $E^\dagger(\lambda, z' + h)$ can be approximated by $E(\lambda, z' + h)$ using Born Approximation. Therefore, δE can be expressed in terms of $E(\lambda, z')$. In [18] it is shown that:

$$\begin{aligned} \delta E(\lambda, h, \omega) &= \frac{-j\omega\mu}{2u_0 E_p(\lambda, 0, \omega)} \int_0^{\infty} E^2(\lambda, z', \omega) \delta\sigma(z') dz' \\ &= \frac{e^{u_0 h}}{aI(\omega) J_1(\lambda a)} \int_0^{\infty} E^2(\lambda, z', \omega) \delta\sigma(z') dz' \end{aligned} \quad (6.13)$$

where we used (6.4) to substitute for E_p

If we discretize $\sigma(z')$, such that conductivity σ is assumed constant at a value of σ_i in the region ($z_i \leq z \leq z_{i+1}$), then (6.13) will be of the form:

$$\delta E(\lambda, h, \omega) = \frac{e^{u_0 h}}{aI(\omega) J_1(\lambda a)} \underline{f}^T \underline{g} \quad (6.14)$$

where:

$$g_i = \delta\sigma(z_i) \quad (6.15)$$

$$f_i(\lambda, \omega) = \int_{z_i}^{z_{i+1}} E^2(\lambda, z', \omega) dz' \quad (6.16)$$

The evaluation of f_i in (6.16) is given in [18] as follows: The general solution of E in i 'th layer is a combination of up-going and down-going plane waves. So we can express $E(\lambda, z, \omega)$ as follows:

$$E(\lambda, z, \omega) = A_i e^{u_i(z-z_i)} + B_i e^{-u_i(z-z_i)} \quad (6.17)$$

A_i and B_i are given by recursive formulas as

$$A_i = B_i e^{-2u_i h_i} \frac{Z^{i+1} - Z_i}{Z^{i+1} + z_i} \quad (6.18)$$

$$B_{i+1} = B_i e^{-u_i h_i} \frac{Z^{i+1} + Z_i}{Z^{k+1} + z_k} \quad (6.19)$$

Z_i , and Z^i are given in (6.6) and (6.7).

Taking the inverse Hankel-transform of (6.14), we get:

$$\delta E(R, h, \omega) = \frac{1}{aI(\omega)} \int_0^\infty \frac{e^{u_0 h}}{J_1(\lambda a)} \lambda J_1(\lambda R) \underline{f}^T \underline{g} d\lambda \quad (6.20)$$

$$= \underline{F}_e^T \underline{g} \quad (6.21)$$

where: $F_{e_i} = \frac{1}{aI} \int_0^\infty \frac{e^{u_0 h}}{J_1(\lambda a)} \lambda J_1(\lambda R) f_i d\lambda$

To derive a similar equation for the case when measured data are H_r and H_z we use equations (6.1a) and (6.1b).

From (6.1a) and (6.20), and noting that $e^{u_0 h}$ in (6.20) is actually $e^{u_0(h+z)}|_{z=0}$, we get:

$$\delta H_r(R, h, \omega) = \frac{-j}{\omega \mu a I(\omega)} \int_0^\infty \frac{u_0 e^{u_0 h}}{J_1(\lambda a)} \lambda J_1(\lambda R) \underline{f}^T \underline{g} d\lambda \quad (6.22)$$

$$= \underline{F}_r^T \underline{g} \quad (6.23)$$

From (6.1b) and (6.20) we get:

$$\begin{aligned} \delta H_z(R, h, \omega) &= \frac{j}{\omega \mu a I(\omega)} \int_0^\infty \frac{e^{u_0 h \lambda}}{J_1(\lambda a)} \left\{ \frac{1}{r} \frac{\partial}{\partial r} (r J_1(\lambda r)) \right\}_{r=R} \underline{f}^T \underline{g} d\lambda \\ &= \frac{j}{\omega \mu a I(\omega)} \int_0^\infty \frac{e^{u_0 h \lambda}}{J_1(\lambda a)} \lambda^2 J_0(\lambda R) \underline{f}^T \underline{g} d\lambda \quad (6.24) \\ &= \underline{F}_z^T \underline{g} \quad (6.25) \end{aligned}$$

A set of equations representing different measurements for either equation (6.21), (6.23), or (6.25) can be written in matrix form as:

$$F \underline{g} = \underline{d} \quad (6.26)$$

where:

F is a matrix with rows equal to \underline{F}_c^T , \underline{F}_r^T or \underline{F}_z^T

Elements of \underline{d} represent different measurements corresponding to different frequencies (*Parameteric Sounding*) or different receiver locations (*Geometric Sounding*.)

A Hopfield neural network can be developed to solve the integral equation described in (6.26) as shown in Chapter 5.

Radially Inhomogeneous Slab

We assume here that the media consist of cylindrical layers, where layer i has conductivity σ_i , and permittivity ϵ_i , (Figure 6.2). The transmitter is a circular antenna . Receivers are also circular antennas that are located at different positions z_i . In this problem, we are trying to reconstruct permittivity and conductivity of different subannuli of the slab. The inversion problem of cylindrically stratified lossy media is introduced in [10]. The formulation of this problem simulates a deep propagation tool (DPT) used for dielectric logging in a borehole described in Appendix A.

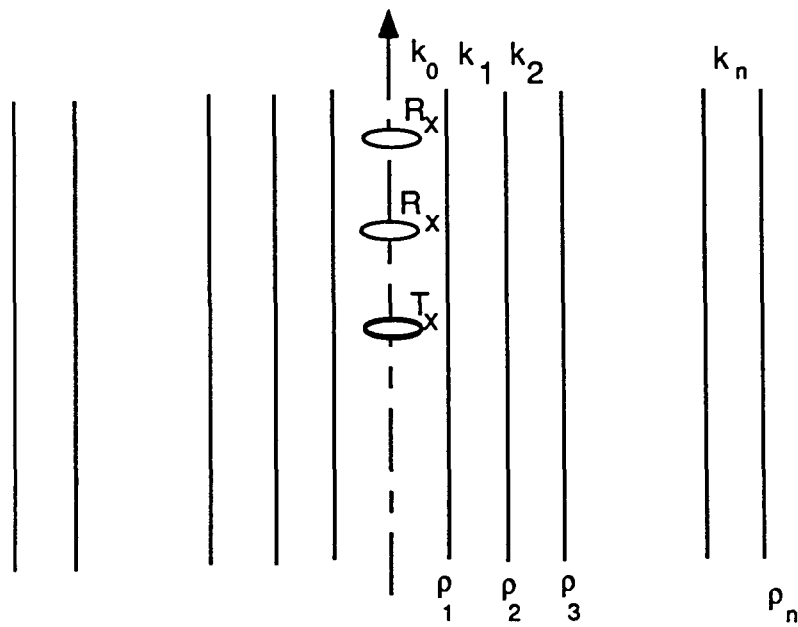


Figure 6.2: Coaxial cylinders model

Forward Problem

We follow here the procedure given by Chew [47] to solve the forward problem. First, consider the solution of the wave equation of a small loop antenna of radius a .

$$\nabla^2 E_\phi + k^2 E_\phi = 0 \quad (6.27)$$

where

$$\nabla^2 E_\phi = -\nabla \times \nabla \times E_\phi$$

$$\begin{aligned} \nabla \times E_\phi &= \frac{1}{\rho} \begin{vmatrix} \hat{\rho} & \rho\hat{\phi} & \hat{z} \\ \frac{\partial}{\partial \rho} & 0 & \frac{\partial}{\partial z} \\ 0 & \rho E_\phi & 0 \end{vmatrix} \\ &= -\frac{\partial E_\phi}{\partial z} \hat{\rho} + \frac{1}{\rho} \frac{\partial}{\partial \rho} (\rho E_\phi) \hat{z} \end{aligned}$$

$$\nabla \times \nabla \times E_\phi = \frac{1}{\rho} \begin{vmatrix} \hat{\rho} & \rho\hat{\phi} & \hat{z} \\ \frac{\partial}{\partial \rho} & 0 & \frac{\partial}{\partial z} \\ -\frac{\partial E_\phi}{\partial z} & 0 & \frac{1}{\rho} \frac{\partial}{\partial \rho} (\rho E_\phi) \end{vmatrix}$$

Therefore the wave equation (6.27) can be written in the form:

$$\left(\frac{\partial^2}{\partial \rho^2} + \frac{1}{\rho} \frac{\partial}{\partial \rho} - \frac{1}{\rho^2} + \frac{\partial^2}{\partial z^2} + k^2 \right) E_\phi = 0 \quad (6.28)$$

Kong [48] gave the solution of equation (6.28) as:

$$E_\phi = \begin{cases} \int_{-\infty}^{\infty} A J_1(\gamma \rho) e^{jk_z z} dk_z & \rho \leq a \\ \int_{-\infty}^{\infty} B H_1^{(1)}(\gamma \rho) e^{jk_z z} dk_z & \rho \geq a \end{cases} \quad (6.29)$$

where: $\gamma = \sqrt{k^2 - k_z^2}$

Calculating $H = (1/j\omega\mu)\nabla \times E$ and matching boundary conditions on $\rho = a$, such that E_ϕ is continuous, and equating $\nabla \times H_z$ to the current density \underline{J} in the loop, where \underline{J} is given by:

$$\underline{J} = \hat{\phi}I\delta(\rho - a)\delta(z)$$

we get [47]

$$E_\phi = \frac{-\omega\mu I a}{4} \int_{-\infty}^{\infty} dk_z e^{jk_z z} J_1(\gamma_1 a) H_1^{(1)}(\gamma_1 \rho) \quad \rho \geq a \quad (6.30)$$

There is an analogy between this problem and a transmission line, as shown by Wait [49] (Figure 6.3). The voltage at any point is the sum of incident and reflected voltages. The field will be a spectrum of cylindrical waves of Hankel and Bessel functions [47]. Hankel function is unbounded at the origin and Bessel function is bounded at the origin. Therefore, reflected waves are assumed to be Bessel functions and incident waves are assumed to be Hankel functions, (Figure 6.4). We assume that the transmission coefficient from section (m-1) to section m is $T_{m-1,m}$, and the reflection coefficient from section (m-1) to section (m) is $\Gamma_{m,m-1}$.

At section m, the total field will be a summation of Bessel and Hankel functions, which can be written in the form:

$$A_m [H_1^{(1)}(\gamma_m \rho) + B_m J_1(\gamma_m \rho)]$$

The Hankel wave at section m is proportional to the sum of incident Hankel wave from section (m-1) to m, and reflected Bessel wave from m to (m-1), therefore:

$$A_m = A_m B_m \Gamma_{m,m-1} + A_{m-1} T_{m-1,m} \quad (6.31)$$

Similarly for the Bessel wave in section m, we get:

$$A_m B_m = A_{m+1} B_{m+1} T_{m+1,m} + A_m \Gamma_{m,m+1} \quad (6.32)$$

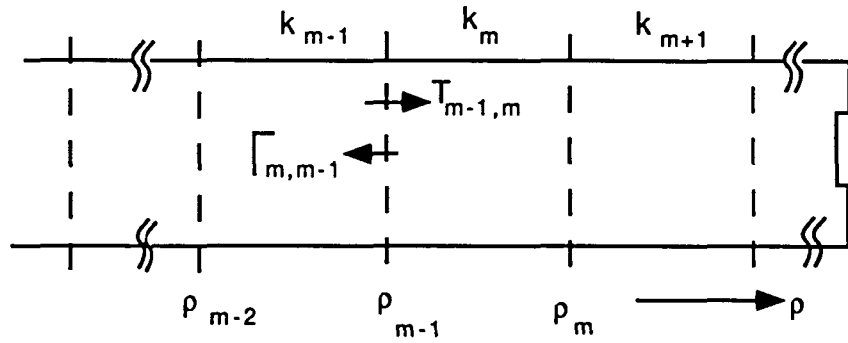


Figure 6.3: Transmission line analogy

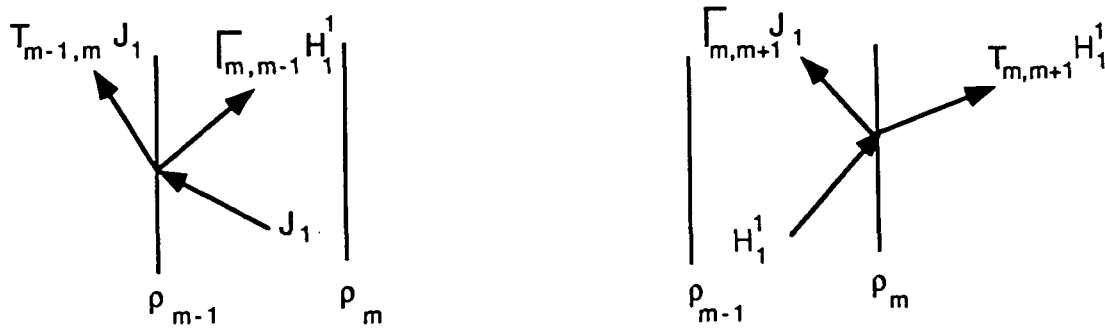


Figure 6.4: Transmission and reflection of Hankel and Bessel waves

From (6.31)

$$\begin{aligned} A_m &= \frac{A_{m-1}T_{m-1,m}}{1 - B_m\Gamma_{m,m-1}} \\ &= A_1 \prod_{m=2}^n \frac{T_{m-1,m}}{1 - B_m\Gamma_{m,m-1}} \end{aligned} \quad (6.33)$$

From (6.32), and (6.33)

$$\begin{aligned} B_m &= \Gamma_{m,m+1} + \frac{A_{m+1}}{A_m} B_{m+1} T_{m+1,m} \\ &= \Gamma_{m,m+1} + \frac{T_{m,m+1} T_{m+1,m}}{1 - B_{m+1} \Gamma_{m+1,m}} \end{aligned} \quad (6.34)$$

Equations (6.33), (6.34) give the recursive relations for A_m , and B_m respectively.

Therefore, we can determine all A_m and B_m in terms of A_1, B_n , where:

$A_1 = J_1(\gamma_1 a)$, and a is the radius of antenna

$B_n = 0$ because there is no reflection.

We are left with determining $T_{m+1,m}, T_{m,m+1}, \Gamma_{m,m+1}$, and $\Gamma_{m,m-1}$.

From (6.30), $E_{m\phi}$, the electric field in section m can be given by [47]:

$$E_{m\phi} = \frac{-\omega\mu I a}{4} \int_{-\infty}^{\infty} dk_z e^{jk_z z} A_m [H_1^1(\Gamma_m \rho) + B_m J_1(\Gamma_m \rho)] \quad (m \leq n) \quad (6.35)$$

From continuity of E_ϕ at R_{m-1} , (Figure 6.4):

$$\begin{aligned} \mu_m [J_1(\gamma_m R_{m-1}) + \Gamma_{m,m-1} H_1^{(1)}(\gamma_m R_{m-1})] = \\ \mu_{m-1} T_{m,m-1} J_1(\gamma_{m-1} R_{m-1}) \end{aligned} \quad (6.36)$$

From continuity of H_z , where H_z is given by:

$$H_z = \frac{1}{j\omega\mu} \frac{1}{\rho} \frac{\partial}{\partial \rho} (\rho E_\phi)$$

we get:

$$\begin{aligned} \gamma_m J_0(\gamma_m R_{m-1}) + \Gamma_{m,m-1} H_0^{(1)}(\gamma_m R_{m-1}) = \\ \gamma_{m-1} T_{m,m-1} J_0(\gamma_{m-1} R_{m-1}) \end{aligned} \quad (6.37)$$

Equations(6.36) & (6.37) are two equations in $T_{m,m-1}, \Gamma_{m,m-1}$, and we can similarly get two equations in $T_{m,m+1}, \Gamma_{m,m+1}$. Knowing $T_{m,m-1}, \Gamma_{m,m-1}, T_{m,m+1}$, and $\Gamma_{m,m+1}$, we can get A_m, B_m from (6.33) and (6.34), and therefore, we can get $E_{m\phi}$ from (6.35)

Inverse Problem

The formulation and numerical solutions of the corresponding inverse problems are given in [10]. The algorithm can be summarized as follows:

For a circular loop antenna, the current density \underline{J} is given by:

$$\underline{J} = I \delta(\rho - \rho') \delta(z - z')$$

The wave equation with permittivity ϵ_c^0 is :

$$\nabla^2 E_\phi^0 - \frac{1}{\rho^2} E_\phi^0 + k_0^2 \epsilon_c^0 E_\phi^0 = -j\omega\mu I \delta(\rho - \rho') \delta(z - z') \quad (6.38)$$

The Green's function for this equation is the solution of:

$$\nabla^2 G^0 - \frac{1}{\rho^2} G^0 + k_0^2 \epsilon_c^0 G^0 = -\frac{1}{\rho} \delta(\rho - \rho') \delta(z - z') \quad (6.39)$$

Therefore,

$$E_\phi^0 = j\omega\mu I a G^0 \quad (6.40)$$

The problem is to solve for the configuration $\epsilon_c(\rho)$, knowing the field $E^0(\rho, k_z)$, corresponding to configuration $\epsilon^0(\rho)$, which is derived from the forward model, and measurements of the field $E(R, z)$ at radius R , and locations z_i .

From (6.40)

$$E^0(\rho, z) = j\omega\mu_0 I a G^0(\rho, a, z) \quad (6.41)$$

$$E(R, z) = j\omega\mu_0 I a G(R, a, z) \quad (6.42)$$

where G, G^0 are Green's functions corresponding to ϵ, ϵ^0 respectively.

From (6.35):

$$G(R, z) = \frac{j}{4} \int_{-\infty}^{\infty} dk_z e^{jk_z z} A_1 [H_1^{(1)}(\gamma_1 R) + B_1 J_1(\gamma_1 R)] \quad 0 \leq R \leq R_1 \quad (6.43)$$

and $A_1 = J_1(\gamma_1 a)$

$$G^0(\rho, z) = \frac{j}{4} \int_{-\infty}^{\infty} dk_z e^{jk_z z} A_m [H_1^{(1)}(\Gamma_m \rho) + B_m J_1(\Gamma_m \rho)] \quad R_{m-1} \leq \rho \leq R_m \quad (6.44)$$

As shown in Chapter 3, the scattered field is given by:

$$E_\phi^s = \int_{\text{volume}} G^0(\underline{r} - \underline{r}') k_0^2 \delta\epsilon_c E_\phi(\underline{r}') d\underline{r}'$$

where: $\delta\epsilon_c = \epsilon_c - \epsilon_c^0$

Therefore:

$$E(\rho, z) - E^0(\rho, z) = \int_{z'=-\infty}^{\infty} \int_{\rho=R_I}^{R_0} G^0[(\rho - \rho'), (z - z')] k_0^2 \delta\epsilon_c E_\phi(\rho', z') d\rho' dz' \quad (6.45)$$

$$G(\rho, a, z) - G^0(\rho, a, z) = \int_{\rho=R_I}^{R_0} k_0^2 \delta\epsilon_c d\rho' \underbrace{\int_{z'=-\infty}^{\infty} dz' G^0(\rho, \rho', z - z') G(\rho', a, z')}_{\text{convolution}} \quad (6.46)$$

where, R_I is the inner diameter of the slab, and R_o is the outer diameter.

If we take Fourier transform of the above equation, we obtain:

$$g(\rho, a, k_z) - g^0(\rho, a, k_z) = 2\pi k_0^2 \int_{R_I}^{R_o} d\rho' \delta\epsilon_c g(\rho', a, k_z) g^0(\rho, \rho', k_z) \quad (6.47)$$

Considering a receiver of radius R , we get:

$$g(R, a, k_z) - g^0(R, a, k_z) = 2\pi k_0^2 \int_{R_I}^{R_o} d\rho' \delta\epsilon_c g(\rho', a, k_z) g^0(R, \rho', k_z) \quad (6.48)$$

If $\delta\epsilon$ is small enough, then g in the integral of equation (6.48) can be replaced by g^0 (using Born approximation), and we have

$$g(R, a, k_z) - g^0(R, a, k_z) = 2\pi k_0^2 \int_{R_I}^{R_o} d\rho' \delta\epsilon_c(\rho') g^0(\rho', a, k_z) g^0(R, a, k_z) \quad (6.49)$$

Equation (6.49) can be written in the form

$$h_c(k_z) = \int_{R_I}^{R_o} d\rho' Q_c(\rho') K_c(\rho, k_z) \quad (6.50)$$

where:

$$h_c(k_z) = g - g^0$$

$$Q_c(\rho') = 2\pi k_0^2 \delta\epsilon_c$$

$$K_c(\rho, k_z) = g^0(\rho', a, k_z) g^0(R, a, k_z)$$

Subscript c indicates that the quantity is complex.

Equation(6.50) can be written in discretized form using a set of N basis functions $R_i(\rho)$, as follows:

$$F_c \underline{V}_c = \underline{h}_c \quad (6.51)$$

where:

$$h_i = h_c(k_{zi}), i = 1, 2, \dots, M$$

$$\sum_{i=1}^N V_c R_i(\rho) = Q_c(\rho)$$

$$F_{cij} = \int_{R_i}^{R_o} K_c(\rho, k_{zi}) R_j(\rho) d\rho$$

Equation (6.51) can be changed to a Fredholm integral equation form with real variables of the form:

$$FV = \underline{h} \quad (6.52)$$

where:

$$h_i := \Re\{h_{cj}\} \quad i = 2j - 1, \quad j = 1, 2, \dots, M$$

$$:= \Im\{h_{cj}\} \quad i = 2j, \quad j = 1, 2, \dots, M$$

$\Re\{h_{cj}\}$ is the real part of h_{cj} , and $\Im\{h_{cj}\}$ is the imaginary part.

$$V_i := \Re\{V_{ci}\} \quad i = 1, 2, \dots, N$$

$$:= \Im\{V_{c(i-N)}\} \quad i = N + 1, N + 2, \dots, 2 * N$$

$$F_{cij} := \begin{cases} \Re\{F_{cij}\} & i = 1, 3, \dots \quad 1 \leq j < N \\ -\Im\{F_{ci(j-N)}\} & i = 1, 3, \dots \quad N < j < 2 * N \\ \Im\{F_{cij}\} & i = 2, 4, \dots \quad 1 \leq j < N \\ \Re\{F_{ci(j-N)}\} & i = 2, 4, \dots \quad N < j < 2 * N \end{cases}$$

Another method for converting (6.51) to a real valued equation, shown in [20], consists of using only amplitude measurements of the scattered electric field. This results in

$$\int_{R_I}^{R_o} d\rho' Q_c(\rho') K_c(\rho', k_z) = \delta g_c^0(k_z) \quad (6.53)$$

$$\text{with } \Re\left\{\frac{\delta g^0}{g^0}\right\} = \delta \log |g^0|$$

$$\therefore \int_{R_I}^{R_o} d\rho' \left\{ \Re\left\{\frac{K_c}{g^0}\right\} \delta\epsilon(\rho) - \Im\left\{\frac{K_c}{g^0}\right\} \frac{\delta\sigma(\rho)}{\omega\epsilon_0} \right\} = \delta \log |g^0| \quad (6.54)$$

which is in the form of a Fredholm equation.

Expressing $\delta\epsilon$, and $\frac{\delta\sigma(\rho)}{\omega\epsilon_0}$ in the form of summation of basis functions R_i , we have

$$\delta\epsilon = \sum_{i=1}^N V_{\epsilon_i} R_i \quad (6.55)$$

$$\frac{\delta\sigma}{\omega\epsilon_0(\rho)} = \sum_{i=1}^N V_{\sigma_i} R_i \quad (6.56)$$

Equation (6.54) can be written in the form:

$$FV = \underline{h}$$

where:

$$h_i = \delta \log |g^0(k_{z_i})|$$

$$V_i = \begin{cases} V_{\epsilon_i} & i = 1, 2, \dots, N \\ V_{\sigma_{(i-N)}} & i = N + 1, N + 2, \dots, 2 * N \end{cases}$$

$$\begin{aligned} F_{ij} &= \int_{R_I}^{R_o} \Re\left\{\frac{K_c(\rho', k_{z_i})}{g^0}\right\} R_j d\rho' & 1 \leq j \leq N \\ &= \int_{R_I}^{R_o} -\Im\left\{\frac{K_c(\rho', k_{z_i})}{g^0}\right\} R_{(j-N)_k} d\rho' & N < j \leq 2 * N \end{aligned}$$

Summary of Algorithm

The step by step procedure for performing the inversion is given below.

1. Obtain measurements of $E_\phi(R, z)$ at different locations 'z'.
2. Normalize $E_\phi(R, z)$ to get $G(R, z)$ as in (6.42).
3. Compute Fourier transform to get $g(R, a, k_z)$.
4. Assume initial guess for complex permittivity ϵ_c .
5. From the forward model get $g^0(\rho, a, k_z)$ at n points of radius ρ .
6. For complex valued measurements, substitute in the following equation:

$$g(R, k_z) - g^0(R, k_z) = 2\pi k_0^2 \int_{R_I}^{R_o} d\rho' \delta\epsilon_c(\rho') g^0(\rho', k_z) g^0(R, k_z)$$

and change the equation in terms of real variables which represent the real and imaginary parts of the complex variables.

For the case of real valued amplitude measurements only, use the following equation:

$$\delta \log |g^0| = 2\pi k_0^2 \int_{R_I}^{R_o} d\rho' \Re\{g^0(\rho', k_z) \delta\epsilon_c\}$$

7. Cast the integral equation in a discretized form.
8. Use neural network implementation as shown in Chapter 5 to obtain solution for ϵ_c .
9. Use the obtained ϵ_c as initial guess, and go to step 4.

Simulation Results

In simulating the forward problem, the frequency was chosen to be 10 MHz. The radii of the transmitter and the receiver were chosen to be 5 cm each. NAG subroutine S17DEF was used to obtain the Bessel function for complex arguments, and NAG subroutine S17DLF was used to obtain the Hankel function for complex arguments.

A modified gradient descent algorithm is used to simulate the minimization of the energy function as described in Chapter 5.

In [10], it was shown that the Lagrange multiplier λ should be chosen to be large in the first few iterations to give more weight to the smoothness constraint. As the iterations progress, the value of λ is decreased in order to expedite minimization of the first term of the energy function. The values for λ in the simulation were chosen to be .005, .003, and .001 for the first three iterations respectively. The parameter λ_1 is chosen to be high. It was chosen to be 10 in order to ensure that ϵ_c takes free space values on the surface of borehole. Figure (6.5) shows the assumed permittivity ϵ , and loss tangent $\frac{\sigma}{\omega\epsilon_0}$. Figures (6.6), and (6.7) show the initial values, and reconstructed values after first, second and third iterations. Figures (6.8), and (6.9) show the reconstructed values using the amplitude of the scattered wave.

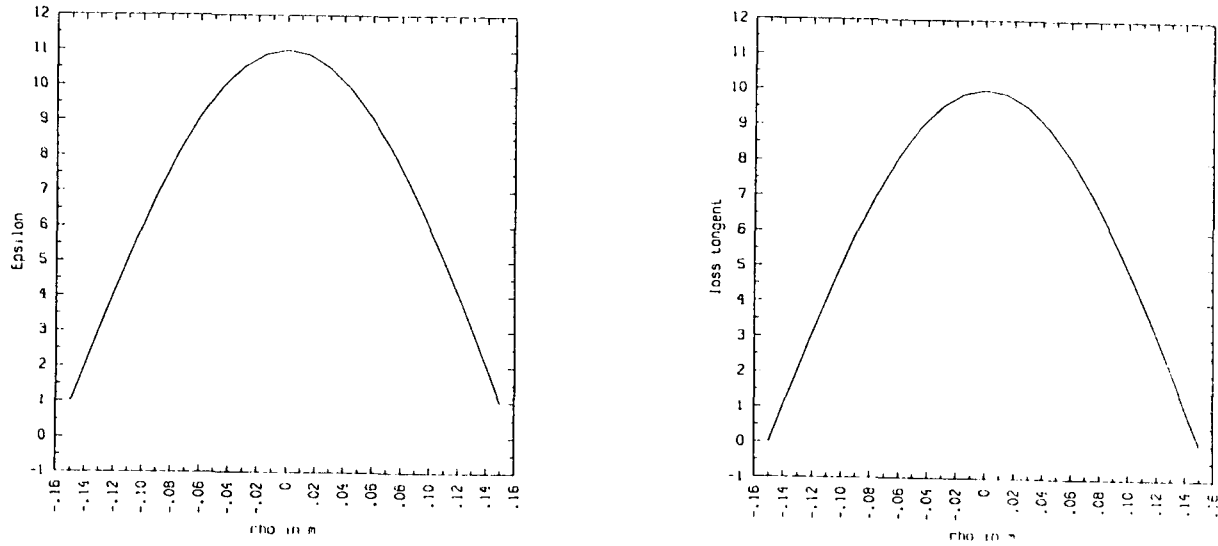


Figure 6.5: True distribution

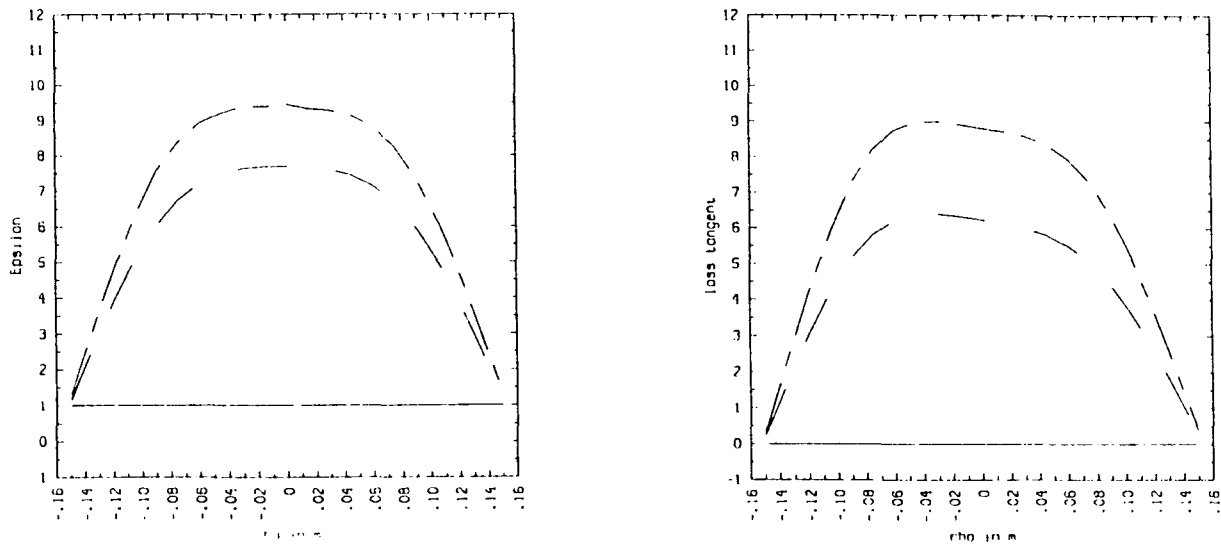


Figure 6.6: Initial value, 1st, and 2nd iterations

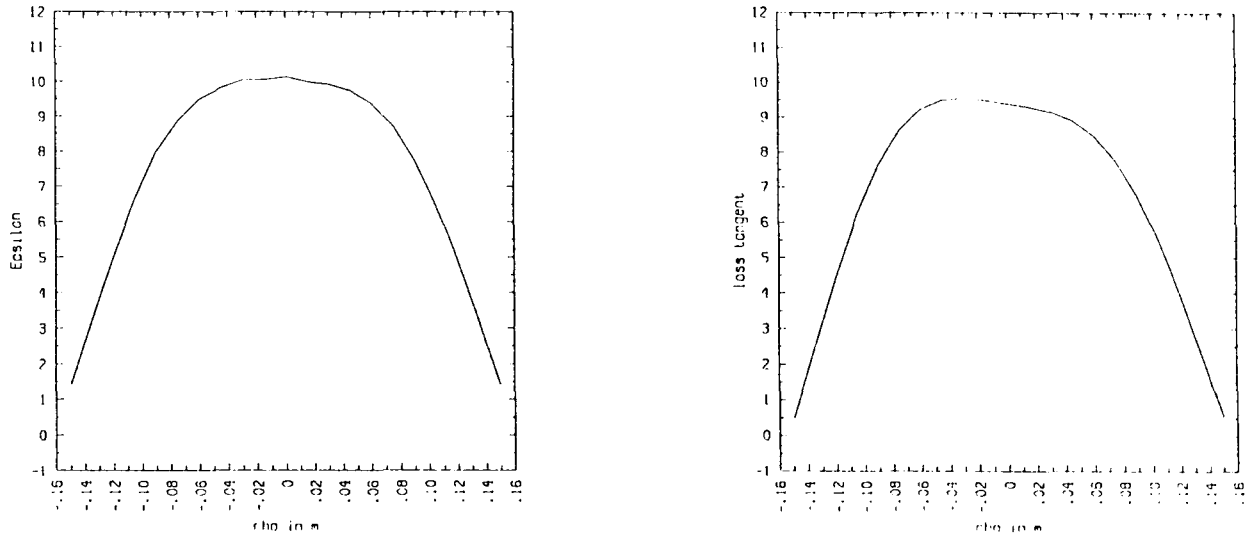


Figure 6.7: 3rd iteration

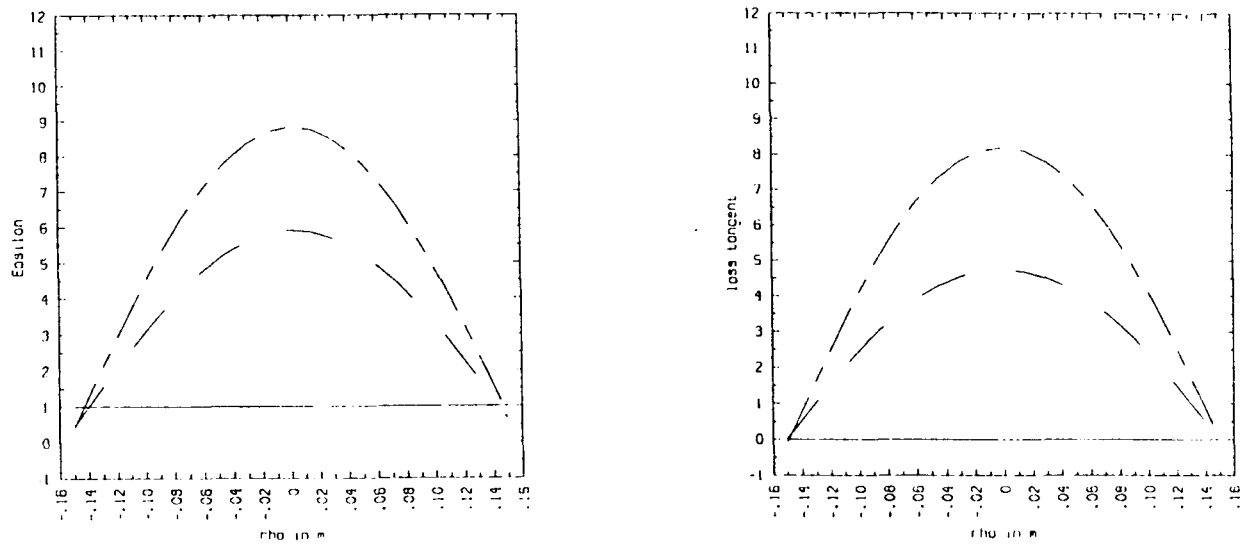


Figure 6.8: Initial value, 1st, and 2nd iterations using amplitude of measurements

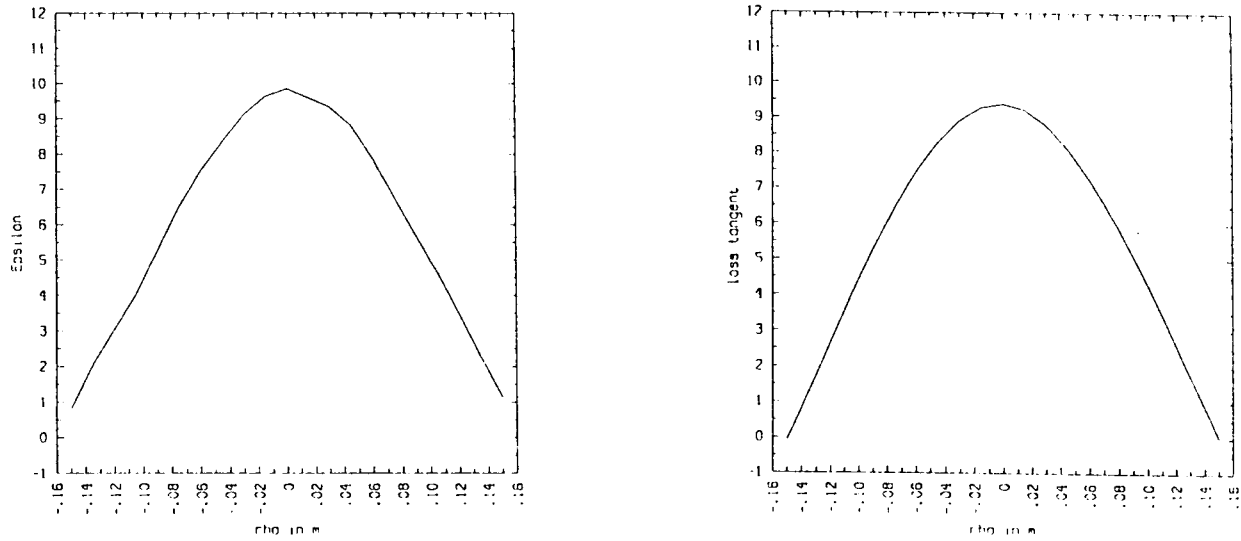


Figure 6.9: 3rd iteration using amplitude of measurements

CHAPTER 7. CONCLUSIONS

This thesis investigates a new approach for solving inverse problems that can be cast in the form of a Fredholm integral equation of the first kind. The approach uses artificial neural networks. Neural networks offer the advantage of exceptional computational ability due to the high degree of parallelism and interconnectivity. This ability makes the neural networks attractive in many fields of engineering and science.

In this thesis, two kinds of neural networks are used for solving inverse problems. The first kind is the multilayer perceptron network. In the training phase, the perceptron is trained using the input and output of the integral equation. Disadvantages of the perceptron include the dependency of the final values of the network weights on the initial values, and the possibility that the network may be trapped in a local minimum. To overcome these disadvantages, different networks are trained, each with different initial weights, and the output is determined by calculating the average of the outputs of all the networks. After completing the training phase, the output of the perceptron is computed when the input data is contaminated with noise. The output is found to converge to the correct solution.

The second kind of neural network used is the Hopfield network. Two applications of electromagnetic inverse problems in geophysics are discussed. The first

application assumes horizontally stratified media, and the second assumes cylindrically stratified media. The formulation in both cases leads to Fredholm integral equation which can be cast in a discretized form assuming the required profile to be the sum of weighted basis functions. The formulation can be developed in terms of the amplitudes of field measurements, thus avoiding the need for phase measurements.

The design of the Hopfield network begins by writing an energy function for the inverse problem. This energy function consists of an error term and constraint terms. Because of the non-uniqueness of the solution, a priori information has to be used in the form of constraints. The types of constraints imposed in the formulation are smoothness constraint, which is reduced progressively during the iterative procedure, and constraints due to boundary conditions. The energy function obtained for the problem is then compared with the energy function of the neural network, thereby deriving the weights of the Hopfield network. Analysis for determining the limits on the parameters of amplifiers for the network to converge to the required solution has been performed.

To overcome the problem of getting trapped in a local minimum, the use of a linear programming Hopfield network connected to the energy minimization network is suggested. Analysis of the stability of both networks is presented, and it is shown the both network will not oscillate. Simulation results, based on the modified gradient descent algorithm, for reconstructing permittivity and conductivity for cylindrically stratified media are presented.

The application of neural networks in solving practical inverse problem will require the use of a large number of neurons. For Hopfield network this necessitates the use of a large number of amplifiers and connecting resistors. However, the imple-

mentation of the network is finding increasing interest with the emergence of optical techniques [50] and VLSI techniques. There are different ways to make the synaptic weights adjustable for VLSI implementation [24]. One method is to implement the weight as an array of resistors and use a memory where each bit controls switching of each resistor. The weights can also be made programmable by implementing the weights as differential amplifiers driven by a current source. EEPROM storage cells are used to inject charges at the floating gate for the current source transistor to control the input current to amplifiers. Thus the differential amplifier will perform as a programmable weight with the value of weight related to trapped charge. Digitally programmable synapses are possible where a weight is implemented by a resistor connected through a switch to the amplifier. The switch is turned on and off with duty cycle controlled by numbers stored in a memory. The average current passing to the amplifier and thus the magnitude of the weight is determined by the ratio of the time the switch is on relative to the whole cycle.

With the growing interest in implementation issues, it is inevitable that the neurocomputer will emerge as the sixth generation computing machine [24], making the proposed approach, for solving inverse problems, very promising.

BIBLIOGRAPHY

- [1] Müller, B., and Reinhardt, J. *Neural Networks: An Introduction*. Berlin: Springer-Verlag, 1990.
- [2] Baumeister, J. *Stable Solution of Inverse Problems*. Braunschweig: Friedr. Vieweg & Sohn, 1987.
- [3] Tihonov, A. N. "Solution of Incorrectly Formulated Problems and the Regularization Method." *Soviet Mathematics* 4 (1963): 1035-1038.
- [4] Groetsh, C. W. *The Theory of Tikhonov Regularization for Fredholm Equations of the First Kind*. Boston: Pitman Advanced Publishing Program, 1984.
- [5] Phillips, D. L. "A Technique for the Numerical Solution of Certain Integral Equations of the First Kind." *J. Ass. Comput. Mach.* 9 (1962): 84-97.
- [6] Habashy, T. M., and Mittra, R. "On Some Inverse Methods in Electromagnetics." *Journal of Electromagnetic waves and applications* 1, 1 (1987): 25-58.
- [7] Habashy, T. M., and Mittra, R. "Review of Some Inverse Methods in Electromagnetics." *J. Opt. Soc. Am.* 4, 1 (January 1987): 281-291.
- [8] Abbott, M. B. *An Introduction to The Method of Characteristics*. New York: American Elsevier, 1966.
- [9] Newton, R. G. "Inversion of Reflection Data for Layered Media: A Review of Exact Methods." *Geophys. J. R. Astr. Soc.* 65 (1981): 191-215.
- [10] Habashy, T. M., Chew, W. C., and Chow, E. Y. "Simultaneous Reconstruction of Permittivity and Conductivity Profiles in a Radially Inhomogeneous Slab." *Radio Science* 21, 4 (1986): 635-645.

- [11] Weston, V. H. "On the Inverse Problem of a Hyperbolic Dispersive Partial Differential Equation." *J. Math. Phys.* 13, 12 (December 1972): 1952-1956.
- [12] Tyras, G. *Radiation and Propagation of Electromagnetic Waves*. New York: Academic Press, 1969.
- [13] Kak, A. C., and Shaney, M. *Principles of Computerized Tomographic Imaging*. New York: IEEE press, 1988.
- [14] Backus, G., and Gilbert, F. "Numerical Applications of a Formalism for Geophysical Inverse Problems." *Geophys. J. R. Astr. Soc.* 13 (1967): 247-276.
- [15] Backus, G., and Gilbert, F. "The Resolving Power of Gross Earth Data." *Geophys. J. R. Astr. Soc.* 16 (1968): 169-205.
- [16] Parker, R. L. "The Inverse Problem of Electrical Conductivity in the Mantle." *Geophys. J. R. Astr. Soc.* 22 (1970): 121-138.
- [17] Parker, R. L. "Understanding Inverse Theory," *Ann. Rev. Earth Planet. Sci.* 5 (1977): 35-64.
- [18] Fullagar, P. K. , and Oldenburg, D. W. "Inversion of Horizontal Loop Electromagnetic Frequency Soundings." *Geophysics* 49, 2 (February 1984): 150-164.
- [19] Coen, S. "Remote Sensing of Dielectric Medium." Ph.D. diss., University of California, Berkeley, 1979.
- [20] Coen, S., Kenneth K. M., and Angelakos, D. J. "Inverse Scattering Technique Applied to Remote Sensing of Layered Media." *IEEE Trans. Antennas Propagat.* AP-29, 2 (March 1981): 298-306.
- [21] Menke, W. *Geophysical Data Analysis: Discrete Inverse Theory*. Orlando: Academic Press Inc., 1984.
- [22] McCulloch, W. S., and Pitts, W. "A Logical Calculus of The Ideas Immanent in the Nervous Activity." *Bulletin of Mathematical Biophysics* 5 (1943): 115-133.
- [23] Griffiths, L. J. "Special Section on Neural Networks: Introduction." *IEEE Trans. Acoust. Speech, Signal Processing* 36, 7 (July 1988): 1107-1109.
- [24] Lee, B. W., and Sheu, B. J. *Hardware Annealing in Analog VLSI Neurocomputing*. Boston: Kluwer Academic Publishers, 1991.
- [25] Lippmann, R. P. "An Introduction to Computing with Neural Nets." *IEEE ASSP Magazine* (April 1987): 4-21.

- [26] Udpa, L., and Udpa, S. S. "Eddy Current Defect Characterization Using Neural Networks." *Materials Evaluation* 48 (March 1990): 342-347.
- [27] Plant, D. C., Nowlan, S. J., and Hinton, G. E. "Experiments on Learning by Back Propagation." *Report CMU-CS-86-126, Computer Science Department Carnegie-Mellon University, Pittsburg, June 1986.*
- [28] Rumelhart, D., McClelland, J., and the PDP Research Group. *Parallel Distributed Processing: Explorations in the Microstructure of Cognition, vol. 1: Foundations*, Cambridge, MA: The MIT Press, 1986.
- [29] Zhou, Y., Chellappa, R., Vaid, A., and Jenkins, B. K. "Image Restoration Using a Neural Network." *IEEE Trans. Acoust. Speech, Signal Processing* 36, 7 (July 1988): 1141-1151.
- [30] Winters, J. H. "Superresolution for Ultrasonic Imaging in Air Using Neural Networks." *IEEE International Conference on Neural Networks* 1 (1988): I.609-I.616.
- [31] Hopfield, J. J. "Neural Networks and Physical Systems with Emergent Collective Computational Abilities." *Proc. Natl. Acad. Sci. USA* 79 (April 1982): 2554-2558.
- [32] Hopfield, J. J. "Neurons with Graded Response Have Collective Computational Properties like those of Two-State Neurons." *Proc. Natl. Acad. Sci. USA* 81 (May 1984): 3088-3092.
- [33] Hopfield, J. J., and Tank, D. W. "'Neural' Computation of Decisions in Optimization Problems." *Biol. Cybern.* 52 (1985): 141-152.
- [34] Hopfield, J. J., and Tank, D. W. "Computing with Neural Circuits: A Model." *Science* 233 (August 1986): 625-633.
- [35] Tank, W. David, and Hopfield, J. J. "Simple 'Neural' Optimization Networks: An A/D Converter, Signal Decision Circuit, and a Linear Programming Circuit." *IEEE Trans. on Circuits and Systems* CAS-33, 5 (May 1986): 533-541.
- [36] Salam, F. M. A., Wang, Y., and Choi, M. "On the Analysis of Dynamic Feedback Neural Nets." *IEEE Trans. on Circuits and Systems* 38, 2 (February 1991): 196-201.
- [37] Kitamura, S., and Qing, P. "An Application of Neural Networks to Solve Fredholm Integral Equations Appearing in Inverse Problems." *4th Japanese Seminar* ✓

on *Nonlinear Problems in Dynamical Systems: Theory and Applications*, Kobe, Oct. 1989.

- [38] Hayward, A. T. J. *Flowmeters: A Basic Guide and Source-Book for users*. London: Macmillan, 1979.
- [39] Wendt, R. E., Jr., ed. *Flow: Its Measurements and Control in Science and Industry*. Vol. 1, Part 2, *Flow Measuring Devices*. Pittsburg: Instrument Society of America, 1974.
- [40] Vogel, C. R. "Numerical Solution of a Non-Linear Ill-Posed Problem Arising in Inverse Scattering." *Inverse Problems* 1 (1985): 393-403.
- [41] Bilgen, M. "Restoration of Noisy Images Blurred by Deterministic or Stochastic Point Spread Function." M.S. thesis, Iowa State University, 1989.
- [42] Hunt, B. R. "The Application of Constrained Least Squares Estimation to Image Restoration by Digital Computers." *IEEE Trans. Comput.* C-22, 9 (September 1973): 805-812.
- [43] Marquardt, D. W. "Solution of Nonlinear Chemical Engineering Models." *Chemical Engineering Progress* 55, 6 (June 1959): 65-70.
- [44] Balanis, C. A. *Antenna Theory: Analysis and Design*. New York: Harper & Row, 1982.
- [45] Ryu, J., Morrison, H. F., and Ward, S. H. "Electromagnetic Fields About a Loop Source of Current." *Geophysics* 35, 5 (October 1970): 862-896.
- [46] Morrison, H. F., Phillips, R. J., and O'Brien, D. P. "Quantitative Interpretation of Transient Electromagnetic Fields over a Layered Half Space." *Geophys. Prosp.* 17 (1969): 82-101.
- [47] Chew, W. C. "Response of a Current Loop Antenna in an Invaded Brorehole." *Geophysics* 49, 1 (January 1984): 81-91.
- [48] Kong, J. A. *Theory of Electromagnetic Waves*. New York: A Wiley-Interscience publication, 1975.
- [49] Wait J. R. *Electromagnetic Waves in Stratified Media*. New York: Pergamon Press Inc., 1962,
- [50] Psaltis, D., and Farhat, N. "Optical Information Processing Based on an Associative-memory Model of Neural Nets with Thresholding and Feedback." *Optics Letters* 10, 2 (February 1985): 98-100.

- [51] Keary, P., and Brooks, M. *An Introduction to Geophysical Exploration*. Oxford: Blackwell Scientific Publication, 1984.
- [52] Keller, G. V., and Frischknecht, F. *Electrical Methods in Geophysical Prospecting*. Oxford: Pergamon Press, 1966.
- [53] Koefoed, O. *Geosounding Principles, 1: Resistivity Sounding Measurements*. Amsterdam: Elsevier Scientific Publishing Company, 1979.
- [54] Banks, R. J. "Geomagnetic Variations and the Electrical Conductivity of the Upper Mantle." *Geophys. J. R. Astr. Soc.* 17 (1969): 457-487.
- [55] Weidelt, P. "The Inverse Problem of Geomagnetic Induction." *Zeitschrift Für Geophysik* 38 (1972): 257-289.
- [56] Zohdy, A. A. R., and Jackson, D. B. "Application of Deep Electrical Soundings for Groundwater Exploration in Hawaii." *Geophysics* 34, 4 (August 1969): 584-600.
- [57] Patra, H. P., and Mallick, K. *Geosounding Principles, 2: Time-Varying Geoelectric Soundings*. Amsterdam: Elsevier Scientific Publishing Company, 1980.
- [58] Koefoed, O., and Biewinga, D. T. "The Application of Electromagnetic Frequency Sounding to Groundwater Problems." *Geoexploration* 14 (1976): 229-241.
- [59] Calvert, T. J., Rau, R. N., and Wells, L. E. "Electromagnetic Propagation: A New Dimension in Logging." *Society of Petroleum Engineers of AIME SPE* 6542, 1977.
- [60] Poley, J. Ph., Nooteboom, J. J., and de Waal, P. J. "Use of V.H.F. Dielectric Measurements for Borehole Formation Analysis." *Log Analyst* 19 (1978): 8-30.
- [61] Freedman, R., and Vogiatzis, J. P. "Theory of Microwave Dielectric Constant Logging Using the Electrmagnetic Wave Propagation Method." *Geophysics* 44, 5 (May 1979): 969-986.
- [62] Huchital, G. S., Hutin, R., Thoraval, Y., and Clark, B. "The Deep Propagation Tool (A New Electromagnetic Logging Tool)." *Society of Petroleum Engineers of AIME SPE* 10988, Sept. 1982.
- [63] Paterson, N., R., and Bosschart, R. A. "Airborne Geophysical Exploration for Ground Water." *Ground Water* 25, 1 (1987): 41-50.

- [64] Overmeeren, R. A. "A Combination of Electrical Resistivity, Seismic Refraction, and Gravity Measurements for Groundwater Exploration in Sudan." *Geophysics* 46, 9 (1981): 1304-1313.
- [65] Frohlich, R. K. "Combined Geoelectrical and Drill-Hole Investigations for Detecting Fresh-Water Aquifers in Northwestern Missouri." *Geophysics* 39, 3 (1974): 340-600.

ACKNOWLEDGEMENTS

Praise be to God, The Cherisher and Sustainer of the worlds; Most Gracious, Most Merciful.

I would like to express my thankfulness for my major professor Dr. L. Udpa, and my co-major professor Dr. S. S. Udpa for their continuous guidance and encouragement during my graduate study at Colorado State University, and Iowa State University.

I wish also to thank Dr. W. Lord, and Dr. R. Thompson for their valuable advice and comments as members of my graduate committee.

I am also appreciative to my friends M. Bilgen, K. Dinçer, J. Gale, and H. El-Arabaty for their help and comments.

The financial support from USAID Project No. 263-0132, the Egypt Water Research Center, and Colorado State University is gratefully acknowledged.

Finally, I would like to thank my parents for their invaluable encouragement and support throughout my education career, and all my family for being always with me while they were thousands of miles away.

APPENDICES

APPENDIX A. GEOPHYSICS

Geophysics is an important field where the application of inverse problems theory plays a major role. The range of geophysical survey methods covers a broad area. The methods that are used for geophysical survey can be divided into two categories, based on whether the source used is natural or artificial.

Geophysical exploration is applied in different fields. These include:

1. The Search of Hydrocarbons
2. Mineral Exploration
3. Engineering Geology
4. Investigation of the Earth's Crust

Geophysical Surveying Methods

The different surveying techniques used in geophysics are discussed in [51]. These techniques are described briefly below.

Seismic Methods

Application of these methods date back to early the 1920s. The method, used to detect surface boundaries, can be used on land or at sea. There are two categories of such methods, namely, *Seismic Reflection*, and *Seismic Refraction* surveying. In

the first method, the travel time of reflected waves from interfaces of subsurfaces are measured. In the second method, the transmitter, and receiver are placed apart and the time of return after traveling through the ground along refracted ray paths is measured. This method can locate interfaces of different seismic velocity bodies and is applicable also for detecting bodies with smoothly varying acoustic impedance.

Gravity Surveying

The basis of gravity surveying methods is based on Newton's law of attraction where the force F between two masses m , and M is given by

$$F = \frac{GmM}{R^2}$$

$$= mg$$

where: G is Gravitational Constant

M is the mass of earth

R is the mean radius of earth

g is the acceleration caused by gravity

An underground zone with a density different from the surroundings will cause a localized perturbation in the gravitational field, known as a gravity anomaly. Gravity methods can be used to locate hydrocarbon traps and sedimentary basins. They can also be used in studying the shape of earth.

Magnetic Surveying

The aim of magnetic surveying is to detect the anomalies in the earth's magnetic field that come from magnetic properties of some of underlying materials.

Magnetic survey can be used on earth , at sea or in the air. With the use of magnetic surveying techniques, information about thick sedimentary cover can be revealed, particularly if some magnetic materials are present within the sedimentary sequence. In the absence of magnetic sediment, the survey data can give information about the crystalline basement.

Electrical Surveying

Resistivity sounding is the most frequently used method in electrical surveying. The method was proposed by Conrad Schlumberger in 1912. This method can be used to investigate the change in resistivity with depth (Vertical Electrical Sounding VES) or lateral change in resistivity(Constant Separation Traversing CST).

The method depends on injecting current into the ground using current electrodes and measuring the potential using potential electrodes [52]. From the values of current and potential we estimate the apparent resistivity. One method of interpreting the apparent resistivity is to draw a curve of apparent resistivity versus a parameter a where a is related to the distance between the current electrodes. Different parts of the curve are matched with master curves [51] prepared for dimensionless quantities (ρ_a/ρ_1) vs. (a/z) , where ρ_a is the apparent resistivity, ρ_1 , and z_1 are the first layer resistivity and depth respectively. A more accurate method is suggested by Koefoed [53]. For a current source I in horizontally stratified media, the potential V at a distance r from the current source can be represented as:

$$V = \frac{\rho_1 I}{2\pi} \int_0^{\infty} K(\lambda) J_0(\lambda r) d\lambda$$

Where, ρ_1 is the upper layer resistivity, and K is the kernel function which can be obtained using recursive relationships.

Defining a function $T_i(\lambda)$ which is called the resistivity transform for layer i

$$T_i(\lambda) = \rho_i K_i(\lambda)$$

an integral equation relationship can be found between apparent resistivity and $T(\lambda)$.

Electromagnetic Methods

Electromagnetic methods are particularly advantageous in geophysics due to the fact that a wide range of frequencies can be employed. This gives considerable flexibility making the method applicable to a wide variety of applications. A survey of the different frequency ranges are described below.

Geophysics Induction Banks [54] worked on determining electrical conductivity of the upper mantle from the geomagnetic spectrum in the range 0.003 to 0.25 cycle/day. Parker [16] worked on the same data of Banks using Backus-Gilbert method. Weidelt [55] worked on similar problems at Ückermünde with period range from 50 sec to 24 hr.

Low Frequency Electromagnetic methods depend on measuring the scattered field from incident waves, for determining the conductivity σ and the permittivity ϵ of the scatterer. For low frequency up to KHz range, the σ term will be dominant in the wave equation, and determining σ can lend insight about the material [56].

Different configurations can be used to obtain conductivity of multilayered earth [57]. The best configuration [58] is to use a transmitter and a receiver of horizontal

coils. For this case we have

$$Z/Z_0 = 1 - \int_{-\infty}^{\infty} R(y)e^{3(x-y)}J_0(e^{x-y})dy$$

where:

Z is the measured mutual impedance of the ratio between receiver voltage and transmitter current.

Z_0 is the mutual impedance in free space.

$x = \ln(r)$, and r is coil spacing.

R is kernel and is given by the following recursive relation:

$$R(\lambda) = R_{0,n}(\lambda)$$

$$R_{(i-1),n}(\lambda) = \frac{v_{i-1,i} + R_{i,n}(\lambda)e^{-2d_i v_i}}{1 + v_{i-1,i}R_{i,n}(\lambda)e^{-2d_i v_i}}$$

while:

$$v_i = \sqrt{\lambda^2 + k_i^2}$$

$$k_i^2 = j\omega\mu\sigma_i$$

$$R_{n,n}(\lambda) = 0$$

The above integration can be performed using digital filter techniques.

Very High Frequency For very high frequency case, the dominant parameter in wave equation is ϵ' , the real part of ϵ_c . A logging tool, *Electromagnetic wave propagation tool* (EPT), was proposed by Calvert and Rau [59] that works at 1.1 GHz. An interesting property was found by Poley et al. [60] which showed that ϵ' is independent of water salinity for frequencies above 200 MHz. This fact is of interest

to the petroleum industry where it is required to differentiate between water and oil, without the knowledge of salinity of water.

The EPT consists of two transmitting and two receiving antennas in a vertical configuration T-R-R-T. The antennas are cavity-backed slot antennas with slot length transverse to the borehole axis.

We can measure the quantity t_{plc} (calculated travel time) where:

$$t_{plc} = \frac{\Delta\phi}{\omega L}$$

$\Delta\phi$ is the phase shift between the two receivers, and L is the distance between them.

The travel time can be related to the properties of the formation by :

$$t_{pl} = \sqrt{\frac{\epsilon'}{2\epsilon_0 c^2} (\sqrt{1 + \tan^2 \delta} + 1)}$$

Where, $c = 3 \times 10^8$ is the velocity of light in a vacuum, and $\tan \delta = \epsilon''/\epsilon'$ is the ratio of real to imaginary parts of permittivity.

In [61], a computer simulation is performed to determine the deviation of t_{plc} from t_{pl} , in the real case where the incident wave is not a plane wave.

High Frequency A device that is used for dielectric logging in a borehole in the MHz range was proposed by Huchital(1980) [62], and is known as DPT (Deep Propagation Tool). Using a relative measurement of phase and amplitude at pairs of receivers, we can derive information of the dielectric constant and conductivity. As the DPT works in a lower frequency range than the EPT, it can achieve deeper investigation than EPT. Analysis of the device is shown in [47]. The DPT can be used to determine the presence of hydrocarbons in zones of variable water resistivity.

APPENDIX B. GROUNDWATER EXPLORATION

The problem of groundwater exploration is addressed using different geophysical methods. Gravity survey methods are used to determine the form and size of porous sedimentary deposits. Seismic reflection techniques provide structural information and seismic refraction techniques provide information on water table, buried channels, and gravel-filled valleys that help to locate groundwater. Magnetic methods are rarely used.

The electrical techniques are the most widely used in hydrology. Resistivity information can be used to detect presence of fresh groundwater, since resistivity depends on salinity.

Application of electromagnetic sounding in groundwater exploration problems seems to be attractive for different reasons [58, 63]:

1. A change in depth information is achieved by changing frequency rather than moving electrodes in resistivity sounding.
2. We avoid problems of introducing the current into ground as this becomes difficult in arid areas.
3. Electromagnetic measurements can be carried out from aircraft, and helicopters.

In [64], 16 vertical electrical soundings were made. In order to solve the equiv-

alence problem (non-uniqueness of interpretation of data), seismic refraction was carried out at some selected places. In [58], electromagnetic sounding was applied in two arid areas in south Tunisia. Comparison between results of EM sounding and drilling showed satisfactory agreement.

In [56], resistivity sounding was applied in the islands of Oahu and Hawaii. On the island of Hawaii, an exploratory well drilled to a depth of 1001 ft (prior to resistivity survey) proved that the well is dry. Interpretation of deep soundings suggested that the minimum depth of a conductive layer, which may represent basalt saturated with fresh water was about 2700 ft.

In [65], a geoelectrical investigation was done in an area of northwestern Missouri, which was previously explored by drill holes. It was found that resistivity depth sounding can partially localize and determine the thickness and depth of near-surface and basal fresh-water bearing gravel bodies in glacial deposits.